State estimation in wall-bounded flow systems. Part 1. Perturbed laminar flows

By JÉRÔME HŒPFFNER[1], MATTIAS CHEVALIER[1,2],
THOMAS R. BEWLEY[3] AND DAN S. HENNINGSON[1,2]

[1]Department of Mechanics, Royal Institute of Technology (KTH), S-100 44 Stockholm, Sweden

[2]The Swedish Defense Research Agency (FOI), SE-172 90, Stockholm, Sweden

[3]Flow Control Lab, Department of MAE, University of California at San Diego, La Jolla, CA 92093-0411, USA

In applications involving the model-based control of transitional wall-bounded flow systems, it is often desired to estimate the interior flow state based on a history of noisy measurements from an array of flush-mounted skin-friction and pressure sensors on the wall. This paper considers this estimation problem, using a Kalman filter based on the linearized Navier–Stokes equations and appropriate stochastic models for the relevant statistics of the initial conditions, sensor noise and external disturbances acting on the system. We show that a physically relevant parameterization of these statistics is key to obtaining well-resolved feedback kernels with appropriate spatial extent for all three types of flow measurement available on the wall. The effectiveness of the resulting Kalman and extended Kalman filters that implement this feedback is verified for both infinitesimal and finite-amplitude disturbances in direct numerical simulations of a perturbed laminar channel flow. The consideration of time-varying feedback kernels is shown to be particularly advantageous in accelerating the convergence of the estimator from unknown initial conditions. A companion paper (Part 2) considers the extension of such estimators to the case of fully developed turbulence.

1. Introduction

The feedback control of fluid flow systems is a problem that has received growing attention in recent years and has been approached in a number of different ways. One approach is to design controls based on physical insight into dominant flow mechanisms, as by the wave superposition principle (see e.g. Thomas 1990). Another approach is to use adaptive or genetic techniques to attempt to learn an effective control strategy by trial and error (see e.g. Lee *et al.* 1997). It is also possible to leverage linear control theory, basing the control algorithm on the linearized Navier–Stokes equations governing small perturbations to the flow system, a mathematical statement of the control objective, and a mathematical model of the relevant statistical properties of the unknown initial conditions, sensor noise and external disturbances acting on the system. The present paper follows this latter approach. Reviews of related flow control efforts can be found in, for instance, Bewley (2001), Gunzberger (1996) and Kim (2003).

The problem of linear model-based feedback control based on noisy measurements can be decomposed into two independent subproblems: (i) the state-feedback (or full-information) control problem, in which full state information is used to determine

effective control feedback; (ii) the state estimation problem, in which measurements are continuously used to 'nudge' a real-time calculation of the flow system in an appropriate manner such that the calculated flow state eventually approximates the actual flow state.

Once both subproblems are solved, we can synthesize them to control a flow based on limited noisy measurements of the flow system. The overall performance of the resulting linear feedback control scheme is limited by the individual performance of the two subproblems upon which it is based. For the application of linear control theory to wall-bounded flows, though encouraging results have been obtained previously on the state-feedback control problem (see, for example, Bewley & Liu 1998; Högberg, Bewley & Henningson 2003), the development of effective state estimation strategies remained, until now, largely an open problem. In the present paper, we therefore focus on the state estimation problem exclusively.

One of the primary challenges of the state estimation problem is that its framing is based centrally on quantities which are challenging to model, namely, the expected statistics of the initial conditions, the sensor noise and the external disturbances acting on the system. The state estimation problem may actually be thought of as a filtering problem; that is, the estimator uses the governing equation itself as a filter to extract, from the available noisy measurements of a small portion of the dynamic system, that component of the measurements which is most consistent with the dynamic equation itself. In other words, the estimator uses the governing equation to extract the signal from the noise, and in the process builds up an estimate of the entire state of the system. The purpose of the estimator at time t is to filter the measurements gathered prior to time t to estimate the instantaneous state of the flow field. The purpose of the state-feedback controller at time t, on the other hand, is to apply forcing to the flow such that the subsequent evolution of the flow, after time t, exhibits favourable characteristics. Thus, the controller is based on a metric defining these favourable characteristics (the objective function), whereas the estimator is based on a model describing, to the extent that they are known, the statistical properties of the unknown quantities affecting the system.

Some attention has been paid in the literature to the creative choice of objective functions for the control problem. Kim & Lim (2000), for example, performed a numerical experiment which applied body forcing via linear feedback everywhere on the interior of a turbulent channel flow. This linear feedback was constructed to cancel exactly the linear coupling term ($\mathscr{C}$ in (2.2)) in the nonlinear simulation, with the result that the turbulent flow relaminarized. This result lends credibility to the idea of using a more sophisticated objective function which targets this linear coupling (more precisely, one which targets the non-normality of the system eigenvectors) rather than using an objective function which simply targets the energy of the flow perturbations directly. The appropriate selection of the objective function is thus seen to be not a trivial problem, and is closely linked to our understanding of the relevant flow physics. The problem of disturbance modelling for the state estimation problem, which is also inherently linked to our understanding of the relevant flow physics, is perhaps even more subtle.

The importance of appropriate disturbance modelling was previously investigated by Jovanović & Bamieh (2001a). In this work, a stochastic disturbance model was proposed which, when used to force the linearized Navier–Stokes equation, led to a simulated flow state with certain second-order statistics (specifically, u_{rms}, v_{rms}, w_{rms}, and the Reynolds stress $-\overline{uv}$) that mimicked, with varying degrees of precision, the statistics from a full direct numerical simulation (DNS) of a turbulent flow at $Re_\tau = 180$.

The present work represents the next natural step in this vein, that is, the development of appropriate disturbance parameterizations that facilitate the calculation of well-resolved feedback kernels for the flow estimation problem that both converge upon grid refinement and eventually decay exponentially with distance from the origin (that is, from the corresponding sensor location). These feedback kernels, in turn, facilitate accurate estimation of the state itself when a simulation of the state estimate is coordinated with wall measurements from an actual flow (or a separate direct numerical simulation thereof). Further, the tuning of this disturbance parameterization allows for the tuning of the spatial extent of the resulting feedback convolution kernels in order to modify the communication architecture required in an 'overlapping decentralized' implementation of the resulting estimator in hardware (that is, large-scale implementation via an interconnected array of identical tiles, each with actuators, sensors and control logic incorporated, that communicate only with their neighbours, as described in detail in Bewley 2001).

It appears as if little has been accomplished to date in terms of the investigation of appropriate disturbance models for specifically the flow estimation problem in the published literature. Bewley & Liu (1998) Joshi, Speyer & Kim (1999) and Högberg *et al.* (2003) all modelled the covariance of the external disturbances at a single wavenumber pair $\{k_x, k_z\}$ in a channel flow with a simple identity matrix after the problem was discretized in the wall-normal direction. This assumption effectively implies a constant variance of disturbances at each gridpoint in the wall-normal direction and zero correlation of the disturbances at different gridpoints above the wall. Unfortunately, this covariance model does not converge to a resolved covariance distribution as the wall-normal grid is refined. We now understand that, as a consequence, this model was responsible for restricting the effectiveness of the resulting estimators in our previous work, and also led to realization problems that required us to limit the number of wall measurements that we could account for while still obtaining convergence of the feedback kernels upon refinement of the numerical grid.

In the present paper, we propose an improved parameterization of the external disturbances (that is, random volume forcing on the interior of the flow domain) that may be used to model the effects of wall roughness, acoustic waves and neglected dynamics, as well as appropriate parameterizations of the unknown initial conditions and sensor noise. This improved disturbance parameterization converges to a continuous function upon grid refinement, and allows us to account for all three flow measurements available at the wall (that is, streamwise and spanwise wall skin friction and wall pressure).

In previous studies, only time-constant feedback kernels have been considered in the estimator. By introducing time-varying feedback kernels into the estimator, the present paper incorporates plausible models of the statistics of the unknown initial conditions on the flow in order to maximize the speed of convergence of the estimator from unknown initial conditions. As a consequence, the initial transients in the estimation error are shown to be greatly diminished.

We design and test an estimator for the early stages of transition in a laminar three-dimensional plane channel flow (again, see Part 2 of this study for the case of fully developed turbulence). After describing the system of interest, we propose a stochastic model for the flow's initial conditions, external disturbances, and sensor noise in §2.4. An appropriate Kalman filter is designed in §2.5 in order to determine suitable estimator feedback. After a discussion of the numerical methods employed, we test the estimator in numerical simulations of the linearized system at isolated wavenumber pairs in §3. We then inverse Fourier transform the estimator feedback

rules determined on a large array of wavenumber pairs to obtain well-resolved spatially localized feedback convolution kernels in physical space for all three of the measurable quantities on the wall (streamwise and spanwise wall skin friction and wall pressure), as discussed in §4.1. The resulting Kalman filter for the entire three-dimensional channel, and an extended Kalman filter that additionally incorporates the nonlinearity of the full system, are tested in direct numerical simulations of the full nonlinear Navier–Stokes system for both infinitesimal and finite-amplitude perturbations of a laminar channel flow in §§4.2 and 4.3.

2. Formulation

2.1. *Flow configuration and governing equations*

This paper considers the three-dimensional flow between two infinite flat plates (at $y = \pm 1$) driven by a pressure gradient in the streamwise (x) direction. Scaling the time variable appropriately, the mean velocity profile is given by $U(y) = 1 - y^2$. For computational efficiency, we model the flow as being periodic in the horizontal directions x and z, using a computational domain of sufficient extent in these directions that this non-physical assumption does not significantly affect the statistics of the flow. This approach allows all variables with spatial variation to be expanded in Fourier series. Thus, the state vector describing the wall-normal velocity $\hat{v}_{mn}(y, t)$ and wall-normal vorticity $\hat{\eta}_{mn}(y, t)$ on the interior of the domain at each wavenumber pair $\{k_x, k_z\}_{mn}$ may be denoted by

$$\hat{q}_{mn}(y, t) = \begin{pmatrix} \hat{v}_{mn}(y, t) \\ \hat{\eta}_{mn}(y, t) \end{pmatrix}.$$

The evolution of the flow can then be written with the linear terms, M and L, on the left-hand side and the nonlinear terms, N, on the right-hand side, in addition to an external forcing term $\hat{e}_{mn}$ to account for unmodelled effects, yielding

$$\underbrace{\frac{\mathrm{d}}{\mathrm{d}t} M\hat{q}_{mn} + L\hat{q}_{mn}}_{\text{Linear dynamics}} = \underbrace{\sum_{\substack{k+i=m \\ l+j=n}} N(\hat{q}_{kl}, \hat{q}_{ij})}_{\text{Nonlinear coupling}} + \underbrace{\hat{e}_{mn}(y, t)}_{\text{External forcing}}, \quad (2.1)$$

where

$$M = \begin{pmatrix} -\Delta & 0 \\ 0 & I \end{pmatrix}, \quad L = \begin{pmatrix} \mathscr{L} & 0 \\ \mathscr{C} & \mathscr{S} \end{pmatrix}. \quad (2.2)$$

For the remainder of this paper (Part 1), the entire derivation is done in Fourier space, so the accent $(\hat{\cdot})$ and subscript $(\cdot_{mn})$ will be dropped for notational clarity. The operators $\mathscr{L}$, $\mathscr{S}$ and $\mathscr{C}$ relate to the Orr–Sommerfeld/Squire equations and are defined as

$$\mathscr{L} = -\mathrm{i}k_x U \Delta + \mathrm{i}k_x U'' + \Delta^2/Re,$$
$$\mathscr{S} = \mathrm{i}k_x U - \Delta/Re,$$
$$\mathscr{C} = \mathrm{i}k_z U'.$$

The Laplacian operator is denoted $\Delta = \mathrm{D}^2 - k^2$, where D and D^2 represent first- and second-order differentiation operators in the wall-normal direction, and $k^2 = k_x^2 + k_z^2$. The Reynolds number Re is based on the centreline velocity and channel half-width. The double convolution sum in (2.1) represents the nonlinear 'triad' interactions. The boundary conditions on v and η correspond to no-slip solid walls

$$v = \mathrm{D}v = \eta = 0 \quad \text{at} \quad y = \pm 1.$$

In the following, the right-hand side of (2.1) will be lumped into a forcing function $f(y, t)$, thereby restricting the flow model to the linear terms, accounting for both the nonlinear terms and the external disturbances with a stochastic model. The resulting flow model can be written as

$$\frac{\mathrm{d}}{\mathrm{d}t} Mq + Lq = Tf(y, t), \tag{2.3}$$

where the operator

$$T = \begin{pmatrix} \mathrm{i}k_x \mathrm{D} & k^2 & \mathrm{i}k_z \mathrm{D} \\ \mathrm{i}k_z & 0 & -\mathrm{i}k_x \end{pmatrix}$$

transforms the forcing $f = (f_1, f_2, f_3)^T$ on the evolution equation for the velocity vector $(u, v, w)^T$ into an equivalent forcing on the $(v, \eta)^T$ system (see e.g. Jovanović & Bamieh (2001*b*) for derivation of this transformation).

2.2. *Measurements*

The choice of the measurements to be taken in order to obtain the state estimate (without knowledge of the initial conditions of the flow) is ultimately a matter of practicality. In the present work, we will consider an idealized problem in which the continuous distributions of streamwise and spanwise skin friction and pressure on the wall are available as measurements in order to estimate the state of the flow away from the wall. This information is mathematically complete in the following sense: if this information is uncorrupted by noise and the external forcing on the system is known exactly, the entire state of the flow (even in the fully turbulent regime, and at any Reynolds number) is uniquely determined by these measurements at the wall in an arbitrarily small neighbourhood of time t (without knowledge of the initial conditions), as shown by Bewley & Protas (2003). However, in any practical problem, the measurements are corrupted by noise, the modelling of the system is not precise, and there are external disturbances on the system which are not accounted for. Thus, in the practical setting, it is essential to filter the measurements appropriately to reconcile the noisy measurements of the system with an approximate dynamic model of the system. The Kalman filter used in the present paper is a mathematically rigorous tool for achieving this reconciliation.

In our previous formulations of the estimator problem, as discussed in Högberg *et al.* (2003), only the feedback gains using the measurement η_y, the first wall-normal derivative of η, were used. In §2.4, we develop an improved formulation based on a more realistic model of the statistics of the external disturbances such that we may now compute well-behaved feedback kernels that converge upon grid refinement for any measurement constructed as a linear combination of the state variables and their derivatives. In particular, the three available measurements at the wall, the streamwise and spanwise wall skin friction and the wall pressure, are related to the quantities v and η in the state model as follows

$$\tau_x = \tau_{xy}|_{wall} = \frac{1}{Re} u_y|_{wall} = \frac{\mathrm{i}}{Re\, k^2} (k_x \mathrm{D}^2 v - k_z \mathrm{D}\eta)|_{wall},$$

$$\tau_z = \tau_{zy}|_{wall} = \frac{1}{Re} w_y|_{wall} = \frac{\mathrm{i}}{Re\, k^2} (k_z \mathrm{D}^2 v + k_x \mathrm{D}\eta)|_{wall},$$

$$p = p|_{wall} = \frac{1}{Re\, k^2} v_{yyy}|_{wall} = \frac{1}{Re\, k^2} \mathrm{D}^3 v|_{wall}.$$

Note that these equations are easily verified using the Taylor series expansions for $v(y)$ and $\eta(y)$ near a solid wall, as written out in, for example, §2.2 of Bewley & Protas

(2003). In the formulation shown in the remainder of §2, for clarity, we focus on the feedback rules related to measurements made at the lower wall only. The extension of this formulation to the case in which measurements are taken at both walls of the channel, as considered in the simulations reported in §3 and §4, is straightforward.

2.3. *Stochastic setting*

As described earlier, the modelling of the relevant statistical properties of the stochastic forcing function f in (2.3), which accounts for the effects of external disturbances on the system, is one of the key steps in the framing of the present estimation problem.

In the present stochastic framework, the mean of any quantity of interest may be obtained using the expectation operator $E[\cdot]$, defined as the average over all possible realizations of the stochastic inputs. In particular, the mean of f is modelled as zero, that is, $E[f] = 0$.

In the present formulation, it is the *covariance* of f that must be modelled carefully. Since f is a continuous function of the spatial coordinate y, the appropriate definition of the covariance in this problem is somewhat abstract, as discussed in detail in Balakrishnan (1976). As shown in Balakrishnan (1976), once this abstraction is made, the resulting Kalman filter in this spatially continuous formulation is found to be analogous to its well-known counterpart in the finite-dimensional setting. In order to proceed with the modelling of the statistics of f, it is necessary to have a clear understanding of what the covariance means in the spatially continuous setting.

In the spatially discrete setting, if u and v are two zero-mean, random vectors of length n_1 and n_2, respectively, their covariance R_{uv} is defined as a matrix of size $n_1 \times n_2$ such that $R_{uv} = E[uv^*]$, where the symbol * applied to a vector or scalar denotes conjugate transpose. The covariance of a zero-mean random vector u is defined as $R_{uu} = E[uu^*]$.

To extrapolate these definitions to the spatially continuous setting (see e.g. Balakrishnan 1976, p. 267), we make use of inner products with arbitrary test functions chosen from the same Hilbert spaces as the random functions we are considering. That is, if ξ and η are two zero-mean random functions in Hilbert spaces H_1 and H_2, respectively, then their covariance $R_{\xi\eta}$ is defined such that

$$\langle x, R_{\xi\eta} y \rangle_1 = E[\langle x, \xi \rangle_1 \langle y, \eta \rangle_2^*] \quad \forall (x, y) \in H_1 \times H_2, \tag{2.4}$$

where $\langle \cdot, \cdot \rangle_1$ and $\langle \cdot, \cdot \rangle_2$ denote appropriate inner products in the Hilbert spaces H_1 and H_2, respectively. Thus, the covariance $R_{\xi\eta}$ is seen to be a linear operator from H_2 to H_1; this is analogous to the spatially discrete setting, in which the covariance is a matrix which when multiplied by a rank n_2 vector results in a rank n_1 vector. Further, if ξ and η are taken to be simple vectors u and v in the above expression, the inner products may be defined using the simple form $\langle x, y \rangle = x^* y$, and the spatially continuous definition of the covariance reduces immediately to the usual definition given in the spatially discrete setting:

$$\left. \begin{aligned} \langle x, R_{uv} y \rangle &= x^* R_{uv} y \\ \langle x, R_{uv} y \rangle &= E[(x^* u)(v^* y)] = x^* E[uv^*] y \end{aligned} \right\} \Rightarrow R_{uv} = E[uv^*].$$

We will subsequently need to express the covariance of a linear transformation of a random process f of known covariance R_{ff}. Letting $g = \mathcal{H} f$ where $\mathcal{H}$ is a linear

differential operator, it follows from (2.4) that

$$\left.\begin{aligned}\langle x, R_{gg}y\rangle &= \mathrm{E}[\langle x, g\rangle\langle y, g\rangle^*] = \mathrm{E}[\langle x, \mathscr{H}f\rangle\langle y, \mathscr{H}f\rangle^*]\\ &= \mathrm{E}[\langle \mathscr{H}^*x, f\rangle\langle \mathscr{H}^*y, f\rangle^*] = \langle \mathscr{H}^*x, R_{ff}\mathscr{H}^*y\rangle\\ &= \langle x, \mathscr{H}R_{ff}\mathscr{H}^*y\rangle\end{aligned}\right\} \Rightarrow R_{gg} = \mathscr{H}R_{ff}\mathscr{H}^*, \quad (2.5)$$

where $\mathscr{H}^*$ denotes the adjoint of $\mathscr{H}$; note that the adjoint of a linear operator $\mathscr{H} : H_1 \to H_2$ with inner products $\langle\cdot, \cdot\rangle_1$ and $\langle\cdot, \cdot\rangle_2$ on H_1 and H_2, respectively, is defined by the equality

$$\langle y, \mathscr{H}x\rangle_2 = \langle \mathscr{H}^*y, x\rangle_1 \quad \forall\{x, y\} \in H_1 \times H_2.$$

A significant feature of the definition of the covariance is its relation to the expected value of the energy. In the spatially discrete setting, defining the energy using an unweighted inner product, we may define the trace such that

$$\mathrm{tr}(R_{uu}) \triangleq \sum_i \langle\delta_{ji}, (R_{uu})_{jk}\,\delta_{ki}\rangle = \sum_i (R_{uu})_{ii}$$
$$= \mathrm{E}[u_1 u_1^* + u_2 u_2^* + \cdots + u_n u_n^*] = \mathrm{E}[\mathscr{E}(u)],$$

where $\mathscr{E}(u)$ denotes the energy of the vector u. In the spatially continuous setting, the corresponding definition is

$$\mathrm{tr}(R_{\xi\xi}) \triangleq \int_\Omega \langle\delta(x-x'), R_{\xi\xi}\delta(x-x')\rangle\,\mathrm{d}x' = \int_\Omega \mathrm{E}\big[\langle\delta(x-x'), \xi(x)\rangle\langle\delta(x-x'), \xi(x))^*\rangle\big]\mathrm{d}x'$$
$$= \mathrm{E}\left[\int_\Omega \xi(x')\xi^*(x')\,\mathrm{d}x'\right] = \mathrm{E}[\mathscr{E}(\xi)].$$

Accounting for a weighting function in the definition of the energy in these relations is straightforward.

2.4. *Models for the stochastic inputs*

The flow system that we desire to estimate is affected by its unknown initial conditions, the unknown external disturbances that disrupt the evolution of the state, and the unknown sensor noise that corrupts the measurements. Since the estimator is intended to converge effectively over a large number of different realizations, a statistical description (mean and covariance) of these unknown quantities may be used to tune the feedback in the estimator design. The estimator which we will design, also known as a Kalman filter, will be optimal in the sense of obtaining the most accurate estimate possible over a large set of realizations of the system in which the initial conditions, external disturbances, and sensor noise have the assumed statistical properties.

2.4.1. *Modelling of the initial conditions*

For the purpose of the present work, we will model the mean of the unknown initial condition as zero (that is, we assume there is no preferred phase in the initial flow structures) and its covariance as S_0. Since the initial condition in the estimator is always zero, S_0 also represents the covariance of the state estimation error at $t = 0$.

We want to design an estimator that performs well over a large range of possible initial conditions. It is natural to assume that the initial conditions are completely 'random', however, we know from our understanding of the flow physics that there is a tendency for some specific types of flow disturbances to be present in any given flow. For example, Tollmien–Schlichting (TS) waves are likely to be present if the environment is characterized by acoustic waves, streaks are likely to be present if the

environment is characterized by high levels of free-stream turbulence, and streamwise vortices are likely to be present if the environment is characterized by wall roughness. The specific initial conditions which we expect to see at each wavenumber pair in a particular problem (though at an unknown phase and amplitude), and for which we would like to tune the estimator to be particularly efficient at capturing, will be denoted here by $s = s_{mn}(y)$.

We will model the initial conditions q_0 at each wavenumber pair as a linear combination of a component q_s of a specified profile s (but with random magnitude and phase) and a component q_r constructed by a random linear combination of the first p eigenmodes $\xi^j = \xi^j_{mn}(y)$, normalized to unit energy, of the system matrix $M^{-1}L$ in (2.3) such that

$$q_s = \theta_0 s, \quad q_r = \frac{1}{p} \sum_{j=1}^{p} \theta_j \xi^j,$$

where the coefficients θ_j, $j \in \{0, \ldots, p\}$ are uncorrelated complex scalar random variables with zero mean and unit variance. The initial condition q_0 is then modelled as a linear combination of these two components such that

$$q_0 = c_1 (c_2 q_s + (1 - c_2)q_r).$$

The design parameter $c_1 > 0$ is used to specify the expected amplitude of the initial conditions at this wavenumber pair, and the design parameter $c_2 \in [0, 1]$ is used to specify the relative importance of the components q_s and q_r in the initial conditions. The corresponding covariance of the unknown initial conditions is given by

$$S_0 = R_{q_0 q_0} = c_1 \left(c_2 R_{ss} + (1 - c_2) \sum_{j=1}^{p} R_{\xi^j \xi^j} \right). \tag{2.6}$$

Note that we expect the energy of the initial conditions at both large wavenumber pairs and small wavenumber pairs to be small. We may account for this in the present model of the initial conditions by allowing c_1 to vary in a wavenumber-dependent fashion. In the present work, we will model this dependence with the function

$$c_1(k_x, k_z) = c_a k_c^2 e^{-k_c^2} \quad \text{with} \quad k_c^2 = (k_x/c_x)^2 + (k_z/c_z)^2,$$

where the design parameters c_x and c_z may be tuned to select the peak of the expected energy of the initial condition in wavenumber space and the design parameter c_a scales the overall amplitude of the initial conditions. Many other assumed forms for $c_1(k_x, k_z)$ are of course also possible, and may be experimented with in future work.

2.4.2. *Modelling of the external disturbances*

We will assume the external disturbance forcing $f = (f_1, f_2, f_3)^T$ in (2.3) to be a zero-mean ($\mathrm{E}[f_j(x, y, z, t)] = 0$) stationary white Gaussian process with auto-correlation

$$\mathrm{E}[f_j(x, y, z, t) f_k(x + r_x, y', z + r_z, t')] = \underbrace{\delta(t - t')}_{\text{Temporal}} \underbrace{Q_{f_j f_k}(y, y', r_x, r_z)}_{\text{Spatial}},$$

where $\delta(\cdot)$ denotes the Dirac δ-function. The assumption of a 'white' time correlation eases the derivation of the equations for the covariance of the state, and is appropriate when the characteristic time scales of the external disturbances are short as compared with the characteristic time scales of the flow system. When this is not the case, the approach developed herein may be extended to incorporate an additional filter
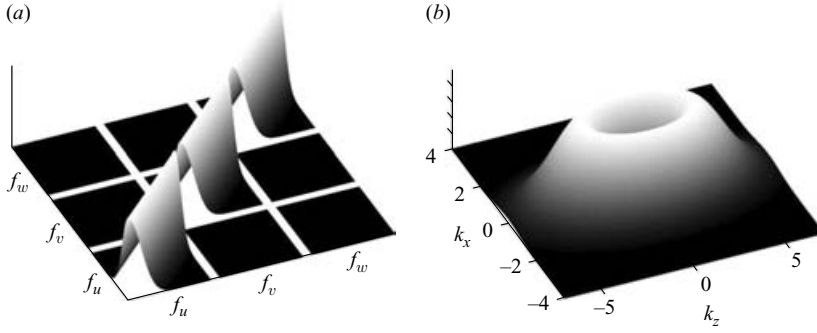
FIGURE 1. (*a*) Sketch of the assumed covariance of the unknown external disturbance f in Fourier space at a single wavenumber pair $\{k_x, k_z\}$, taking $d_y = 0.1$, and (*b*) the variation of the amplitude of this forcing with wavenumbers k_x and k_z, taking $d_x = 0.5$ and $d_z = 3$.

in order to 'colour' the external disturbances with appropriate self-correlation time scales (see e.g. Lewis & Syrmos 1995).

The remaining property to be described is the spatial extent of the two-point one-time auto-correlation of f over the whole domain

$$Q_{f_j f_k}(y, y', r_x, r_z) = E[f_j(x, y, z, t) f_k(x + r_x, y', z + r_z, t)].$$

The corresponding quantity in Fourier space is a covariance operator of the form discussed in §2.3, obtained for any wavenumber pair $\{k_x, k_z\}$ via the following integration over the homogeneous directions

$$R_{f_j f_k}(y, y', k_x, k_z) = \int\int Q_{f_j f_k}(y, y', r_x, r_z) e^{-i(k_x r_x + k_z r_z)} \, dr_x \, dr_z.$$

Our model for the covariance of f assumes that the disturbance has a localized structure in space (i.e. the two-point correlation of the disturbance decays exponentially with distance) and that the correlations between forcing terms on different velocity components are zero. Note that the presence of the wall will introduce correlation between the forcing terms in the streamwise and spanwise directions. Such a correlation is captured by the model used in Part 2 of this study. In the present work, we assume a model for the covariance of the external forcing f which is of a similar form to that assumed for the covariance of the initial conditions by taking

$$R_{f_j f_k}(y, y', k_x, k_z) = d_1 \delta_{jk} \mathcal{M}^y(y, y'),$$

where

$$d_1(k_x, k_z) = d_a k_d^2 e^{-k_d^2} \quad \text{with} \quad k_d^2 = (k_x/d_x)^2 + (k_z/d_z)^2,$$

and the y variation of $R_{f_j f_k}$ is given by the function

$$\mathcal{M}^y(y, y') = e^{-(y-y')^2/(2d_y)}. \tag{2.7}$$

Note that we will denote $R = R_{ff} = \text{diag}(R_{f_1 f_1}, R_{f_2 f_2}, R_{f_3 f_3})$ in the sections that follow. The design parameters d_x and d_z may be tuned to select the peak of the expected energy of the disturbance forcing in wavenumber space, the design parameter d_y governs the width of the two-point correlation of the disturbance in the wall-normal direction, and the design parameter d_a scales the overall amplitude of the disturbance forcing. The variation of $\delta_{jk} \mathcal{M}^y(y, y')$ as a function of y and y', for the three different values of j and the three different values of k, is depicted in figure 1(*a*), and the

variation of $k_d^2 e^{-k_d^2}$ as a function of k_x and k_z is depicted in figure 1(*b*). As with the modelling of the covariance of the initial conditions, many other assumed forms for $d_1(k_x, k_z)$ are also possible, and may be experimented with in future work.

2.4.3. *Modelling of the sensor noise*

Each of the three measurements is assumed to be corrupted by sensor noise, modelled as independent, white (in both space and time), random processes, the amplitude of which is determined by the assumed quality of the sensors. The covariance of the sensor noise vector g can thus be described in Fourier space by a diagonal 3×3 matrix G whose diagonal elements α_i^2 are the variances of the sensor noise assumed to be associated with each individual sensor

$$\boldsymbol{R}_{g_\iota(t), g_\kappa(t')} = \delta_{\iota\kappa} \delta(t - t') \alpha_\iota^2,$$

where $\delta_{\iota\kappa}$ denotes the Kronecker delta. Thus, in the present work, we assume that the sensor noise is uncorrelated in both space and time.

When the signal-to-noise ratio is low, the measured signal must be fed back only gently into the estimator, lest the sensor noise disrupt the estimator. When the signal-to-noise ratio is high, the measured signal may be fed back more aggressively into the estimator, as the fidelity of the measurements can be better trusted. For a given covariance of the initial conditions and external disturbances, the tuning of the assumed overall magnitude of the sensor noise in the Kalman filter design thus provides a natural 'knob' to regulate the magnitude of the feedback into the estimator. Note that an intermediate amount of feedback is desired in the estimator design: if the feedback is too weak, the estimator will not converge very quickly or very accurately, and if the feedback is too strong, it may knock the estimated flow out of the small perturbation neighbourhood assumed in the linear model used in its design.

2.5. *The Kalman filter*

Noting that the Laplacian Δ in the operator M in the forced linear equation (2.3) may be inverted by enforcement of the homogeneous boundary conditions on Dv, we may write

$$\dot{q} = \underbrace{-M^{-1}L}_{A} q + \underbrace{M^{-1}T}_{B} f,$$

and thus the general state-space formulation for the evolution of the flow state $q = q_{mn}(y, t)$ at each wavenumber pair $\{k_x, k_z\}_{mn}$ may be written

$$\left.\begin{aligned} \dot{q} &= Aq + Bf, \quad q(0) = q_0, \\ r &= Cq + g. \end{aligned}\right\} \tag{2.8}$$

Note that q is a continuous function of both the wall-normal coordinate y and time t in this formulation. The measurement vector r is constructed using the matrix $\boldsymbol{C}$, defined here as

$$C = \frac{1}{Re\, k^2} \begin{pmatrix} \mathrm{i}k_x \mathrm{D}^2|_{wall} & -\mathrm{i}k_z \mathrm{D}|_{wall} \\ \mathrm{i}k_z \mathrm{D}^2|_{wall} & \mathrm{i}k_x \mathrm{D}|_{wall} \\ \mathrm{D}^3|_{wall} & 0 \end{pmatrix}.$$

This matrix extracts the two components of wall skin friction and the wall pressure from q.

We now build an estimator of the analogous form

$$\dot{\check{q}} = A\check{q} - v, \quad \check{q}(0) = 0, \\ \check{r} = C\check{q}, \qquad \Big\}$$
(2.9)

with feedback

$$v = L\tilde{r} = L(r - \check{r}).$$
(2.10)

Kalman filter theory, combined with the models outlined in §2.4 for the relevant statistics of the unknown initial conditions q_0, the unknown external forcing f, and the unknown sensor noise g, provides a convenient and mathematically rigorous tool for computing the feedback operator L in the estimator described above such that $\check{q}$ converges to an accurate approximation of q. Note that the volume forcing v used to apply corrections to the estimator is proportional to the 'innovation process' $\tilde{r} = r - \check{r}$, that is, the difference between the measurements of the actual system and the corresponding quantity in the estimator model.

The solution of the Kalman filter problem in the classical finite-dimensional setting is well known (for a succinct presentation, see e.g. Lewis & Syrmos 1995, pp. 463–470). The corresponding operator equations applicable here, though more involved to derive, are completely analogous (see Balakrishnan 1976). Thus, we will not rederive these equations here. The main results, in both the finite-dimensional and infinite-dimensional settings, are:

(*a*) the covariance $S(t) = R_{qq}(t)$ of the flow state $q(t)$ is governed by the Lyapunov equation

$$\dot{S}(t) = AS(t) + S(t)A^* + BRB^*, \quad S(0) = S_0,$$
(2.11)

(*b*) for a given $L(t)$, the covariance $P(t) = R_{\tilde{q}\tilde{q}}(t)$ of the state estimation error $\tilde{q}(t) = q(t) - \check{q}(t)$ is governed by the Lyapunov equation

$$\dot{P}(t) = A_0(t)P(t) + P(t)A_0^*(t) + BRB^* + L(t)GL^*(t), \quad P(0) = S_0,$$
(2.12)

where $A_0(t) = A + L(t)C$, and

(*c*) the value of $L(t)$ which minimizes the expected energy of the state estimation error (that is, which minimizes the trace of $P(t)$) is given by the solution of the differential Riccati equation (DRE)

$$\dot{P}(t) = AP(t) + P(t)A^* + BRB^* - P(t)C^*G^{-1}CP(t), \quad P(0) = S_0,$$
(2.13a)

$$L(t) = -P(t)C^*G^{-1}.$$
(2.13b)

Note that, for a linear time-invariant (LTI) system (that is, for A, B, C, R, G independent of time), the covariance of the estimation error, $P(t)$, and the corresponding feedback which minimizes its trace, $L(t)$, follow a transient near $t = 0$ owing to the effect of the initial condition S_0, eventually reaching a steady state for large t in which $\dot{P}(t) = 0$ and $\dot{L}(t) = 0$. In order to minimize the magnitude of the transient of the trace of $P(t)$, it is necessary to solve the differential Riccati equation given above. If one is only interested in minimizing the trace of $P(t)$ at statistical steady state, it is sufficient to compute time-independent feedback L by solving the algebraic Riccati equation (ARE) formed by setting $\dot{P}(t) = 0$ in (2.13a).

<div align="center">2.6. *Numerical issues*</div>

2.6.1. *Spatial discretization*

In order to actually compute the feedback in this problem, it is necessary to discretize the DRE given in operator form in (2.13) and solve this equation in the finite-dimensional setting. In order to be relevant for the PDE problem of interest, the resulting feedback gains must converge to continuous functions as the numerical grid is refined.

Thus, to proceed, we first need to build the discrete counterparts of the system operators A, B, C, and their respective adjoints as well as the disturbance covariances R, G, and S_0. In the present work, the discrete operators are obtained through enforcement of the Orr–Sommerfeld/Squire equations at each point of a Gauss–Lobatto grid using a Chebyshev collocation scheme, taking

$$f_i = f(y_i), \quad y_i = \cos\frac{i\pi}{N} \quad (i = 0, \dots, N),$$

where $N+1$ is the number of gridpoints in the wall-normal direction. The discrete operators and differentiation matrices are determined using the spectral Matlab Differentiation Matrix Suite of Weideman & Reddy (2000). In particular, this suite provides fourth-order differentiation matrices invoking clamped boundary conditions ($f(\pm 1) = f'(\pm 1) = 0$), using the procedure suggested by Huang & Sloan (1993), to give an Orr–Sommerfeld matrix with satisfactory numerical properties, avoiding unstable or lightly damped spurious eigenmodes. The first-order, second-order, and third-order differentiation matrices so obtained, denoted D^1, D^2 and D^3, respectively, are combined according to the equations given previously to compute the discrete matrices A, B, and C in a straightforward fashion. The calculations reported in this paper use, where needed, the discrete definition for the adjoint of a matrix, that is, its conjugate transpose. The integration weights $W(y_j)$ for the Chebyshev grid with the Gauss–Lobatto collocation points are computed using the algorithm from Hanifi, Schmid & Henningson (1996). These weights provide spectral accuracy in the numerical integration used to assemble the energy measure matrix Q.

2.6.2. *Solution of the DRE*

The calculation of the differential Riccati equation (DRE) is accomplished in this work using the Chandrasekhar algorithm developed by Kailath (1973). This elegant algorithm solves a factored form of the DRE at the heart of the Kalman filter as given by the spatial discretization of the operator equations in (2.13a)–(2.13b). It is particularly efficient when these factors are of low rank, which happens to be the case in the present study.

The main idea in the Chandrasekhar algorithm is to solve an evolution equation for a factored form of the time derivative of the estimation error covariance matrix, $\dot{P}(t)$. Since it is symmetric, $\dot{P}(t)$ can be factored as

$$\dot{P} = L_1 L_1^* - L_2 L_2^* = YHY^*, \quad Y = \begin{pmatrix} L_1 & L_2 \end{pmatrix}, \quad H = \begin{pmatrix} I & 0 \\ 0 & -I \end{pmatrix}, \qquad (2.14)$$

where the rank of $L_1 L_1^*$ is the number of positive eigenvalues of $\dot{P}$ and the rank of $L_2 L_2^*$ is the number of negative eigenvalues of $\dot{P}$.

By spatial discretization of (2.13a), differentiation of both sides, and substitution of the factorization given above, assuming the system is LTI (that is, that A, B, C, R, and G are independent of time), it is straightforward to verify that (2.13a)–(2.13b) is

equivalent to the solution of the following system:

$$
\left.
\begin{aligned}
\dot{\boldsymbol{L}}(t) &= -\boldsymbol{Y}(t)\boldsymbol{H}\boldsymbol{Y}^*(t)\boldsymbol{C}^*\boldsymbol{G}^{-1}, \quad \boldsymbol{L}(0) = -\boldsymbol{P}(0)\boldsymbol{C}^*\boldsymbol{G}^{-1}, \\
\dot{\boldsymbol{Y}}(t) &= (\boldsymbol{A} + \boldsymbol{L}(t)\boldsymbol{C})\boldsymbol{Y}(t), \qquad \boldsymbol{Y}(0)\boldsymbol{H}\boldsymbol{Y}^*(0) = \dot{\boldsymbol{P}}(0),
\end{aligned}
\right\}
\tag{2.15}
$$

where $\dot{\boldsymbol{P}}(0)$ is easily determined from the spatial discretization of (2.12) evaluated at $t = 0$.

The key to the efficiency of this scheme is to exploit the possibility for an accurate low-rank approximation of $\boldsymbol{Y}$. After an eigenvalue decomposition of $\dot{\boldsymbol{P}}(0)$ to determine $\boldsymbol{L}_1$ and $\boldsymbol{L}_2$, we can perform a singular value decomposition of the matrices $\boldsymbol{L}_1\boldsymbol{L}_1^*$ and $\boldsymbol{L}_2\boldsymbol{L}_2^*$ and discard the singular vectors associated with small singular values, constructing an approximation of $\boldsymbol{Y}$ with the remaining singular vectors. In §4, singular values less than 0.01 % of the initial $\dot{\boldsymbol{P}}$ matrix norm were discarded, resulting in a reduction of the rank of $\boldsymbol{Y}$ by approximately 75 %.

In the present work, time integration of the DRE is performed using a standard explicit fourth-order Runge–Kutta scheme. When only constant feedback gains are to be used, we can either march the DRE to steady state using the Chandrasekhar algorithm or solve directly the ARE via standard techniques based on Schur factorization (see Laub 1991).

2.6.3. *Computation of the expected energy*

In the discretized setting, the expected energy of the state $\boldsymbol{q}$ can be extracted from the discrete covariance matrix $\boldsymbol{S}$ by use of the energy measure matrix $\boldsymbol{Q}$ such that $\mathrm{E}[\mathscr{E}(\boldsymbol{q}(t))] = \mathrm{tr}(\boldsymbol{Q}\boldsymbol{S}(t))$, where $\mathscr{E}(\boldsymbol{q}(t))$ denotes the instantaneous energy of the state $\boldsymbol{q}$ at time t. The expected energy of the state estimation error $\tilde{\boldsymbol{q}}$ can be found in a similar manner, $\mathrm{E}[\mathscr{E}(\tilde{\boldsymbol{q}}(t))] = \mathrm{tr}(\boldsymbol{Q}\boldsymbol{P}(t))$.

The time evolution of the expected energy may be computed using the Chandrasekhar method. For example, the expected energy of the state $\boldsymbol{q}$ can be marched forward in time from $\mathrm{E}[\mathscr{E}(\boldsymbol{q}(0))] = \mathrm{tr}(\boldsymbol{Q}\boldsymbol{S}_0)$, its value at $t = 0$, via time integration of $(\mathrm{d}/\mathrm{d}t)\mathrm{E}[\mathscr{E}(\boldsymbol{q})] = \mathrm{tr}(\boldsymbol{Q}\dot{\boldsymbol{S}}(t))$, where $\dot{\boldsymbol{S}} = \boldsymbol{Y}\boldsymbol{H}\boldsymbol{Y}^*$, and where the evolution equation for $\boldsymbol{Y}(t)$ is simply $(\mathrm{d}/\mathrm{d}t)\boldsymbol{Y}(t) = \boldsymbol{A}\boldsymbol{Y}(t)$, with $\boldsymbol{Y}(0)$ determined by the factorization $\boldsymbol{Y}(0)\boldsymbol{H}\boldsymbol{Y}^*(0) = \dot{\boldsymbol{S}}(0)$ and $\dot{\boldsymbol{S}}(0)$ determined by evaluation of (2.11) at $t = 0$. The expected energy of the state estimation error $\tilde{\boldsymbol{q}}$ can be found in a similar manner, marching forward in time from $\mathrm{E}[\mathscr{E}(\tilde{\boldsymbol{q}}(0))] = \mathrm{tr}(\boldsymbol{Q}\boldsymbol{S}_0)$ at $t = 0$ via time integration of $(\mathrm{d}/\mathrm{d}t)\mathrm{E}[\mathscr{E}(\tilde{\boldsymbol{q}})] = \mathrm{tr}(\boldsymbol{Q}\dot{\boldsymbol{P}}(t))$, where $\dot{\boldsymbol{P}} = \boldsymbol{Y}\boldsymbol{H}\boldsymbol{Y}^*$ with, for $\boldsymbol{L}(t)$ specified, $\boldsymbol{Y}(t)$ evolving according to $(\mathrm{d}/\mathrm{d}t)\boldsymbol{Y}(t) = (\boldsymbol{A} + \boldsymbol{L}(t)\boldsymbol{C})\boldsymbol{Y}(t)$ with $\boldsymbol{Y}(0)$ determined by the factorization of $\dot{\boldsymbol{P}}(0)$, which itself is determined by evaluation of (2.12) at $t = 0$.

3. Fourier-space characterization

By Fourier transforming in the x- and z-directions all variables with spatial variation (that is, the state, the disturbances, the measurements and the control), the linearized three-dimensional estimation and control problems completely decouple at each wavenumber pair $\{k_x, k_z\}$, as observed in Bewley & Liu (1998). Thus, the present section characterizes the performance of the estimator derived in the previous section on the linearized system in Fourier space at three individual wavenumber pairs $\{k_x, k_z\} = \{0, 2\}$, $\{1, 0\}$ and $\{1, 1\}$, where this performance is characterized most clearly. In §4, we inverse transform a large array of such feedback gains to physical space, obtaining more readily implementable spatially localized three-dimensional convolution kernels, and consider their effect on direct numerical simulations of the full nonlinear system.
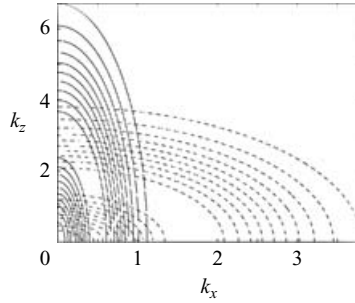
FIGURE 2. Contour plot of the variation of amplitude of the initial conditions, taking $c_x = c_z = 1.7$ (dashed) and external disturbance forcing, taking $d_x = 0.5$, and $d_z = 3$ (solid), as a function of the wavenumbers k_x and k_z. Note that the peak amplitudes are near the design values of k_c and k_d, as defined in §§2.4.1 and 2.4.2, with reduced amplitudes for smaller and larger values of k_c and k_d. The expected covariance of the initial condition is modelled with equal extent in the streamwise and spanwise directions, while the expected covariance of the disturbance forcing is tuned for structures that are elongated in the streamwise direction.

Unless stated otherwise, the results reported are computed for $R = 3000$, a subcritical Reynolds number characterized by transient growth phenomena. The design parameters for the stochastic model for the initial conditions (see §2.4.1) are chosen to be $c_2 = 0.5$, $c_a = 10.9$ and $c_x = c_z = 1.7$. The design parameters for the stochastic model for the external disturbances (see §2.4.2) are chosen to be $d_a = 0.09$, $d_x = 0.5$, $d_z = 3$ and $d_y = 0.1$. The design parameters for the stochastic model for the sensor noise (see §2.4.3) are chosen to be $\alpha_1^2 = \alpha_2^2 = 0.002$ (for the shear-stress measurements) and $\alpha_3^2 = 20$ (for the pressure measurements).

These choices for the design parameters of the stochastic models of the initial conditions, external disturbances and sensor noise are the result of a combination of parametric tuning and physical arguments. For example, the choice $c_2 = 0.5$ reflects a 50 % confidence in the 'specific form' of the assumed statistics of the of the initial conditions. Figure 2 compares the variation with wavenumber of the expected covariance of the initial conditions and disturbance forcing in the model used in this work; these variations excite the wavenumber ranges of interest for the estimation of localized disturbances and the accounting for the early effects of nonlinearity in the transition problem, as studied in §§4.2 and 4.3. The amplitude parameters for the initial condition, c_a, and the external forcing, d_a, are chosen such that the flow energy initially grows and then slightly decays to statistical steady state, for the wavenumber pair showing the greatest potential for transient growth, $\{k_x, k_z\} = \{0, 2\}$.

The initial conditions used for the tests at isolated wavenumber pairs are the 'worst-case' initial conditions at these wavenumber pairs, i.e. the initial conditions that, leveraging the non-normality of the dynamic operator A to the maximum extent possible, lead to the largest possible transient energy growth. Such initial conditions are of particular concern in a flow transition scenario, as described in, e.g. Schmid & Henningson (2001).

The plots in this section show the evolution of the expected value of the energy of both the flow state and the state estimation error for initial conditions, sensor noise and external disturbances distributed as described in the stochastic models presented in §2.4. Thus, these plots can be interpreted as an average over a large number of realizations of these stochastic inputs. They illustrate the effectiveness of the estimator feedback in the presence of the types of disturbance for which the estimator feedback
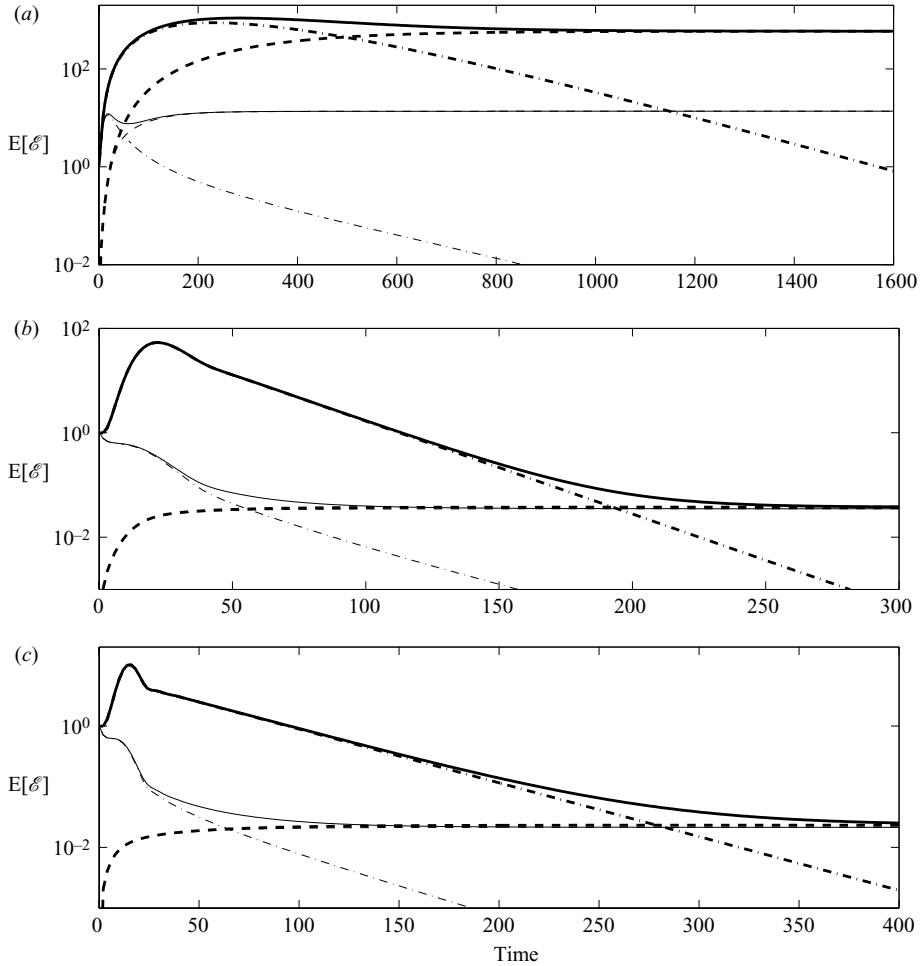
FIGURE 3. Evolution of the expected energy versus time for three flows of interest at three representative wavenumber pairs: (*a*) $\{0, 2\}$, (*b*) $\{1, 1\}$ and (*c*) $\{1, 0\}$. The stochastic inputs driving each simulation are: (solid) initial conditions plus external disturbances, (dashed) external disturbances only, (dot-dashed) initial conditions only; note that each simulation accounts for the effect of sensor noise corrupting the measurements. Thick lines represent the expected energy of the flow disturbance and thin lines represent the expected energy of the estimation error. Note that for $\{1, 1\}$ and $\{1, 0\}$ the thin dashed lines lie under the thick dashed lines.

was designed, namely, uncorrelated zero-mean random Gaussian distributions of the same covariance as specified in the estimator design.

3.1. *Evolution of the expected energy of the flow state and the state estimation error*

Figure 3 shows the evolution of both the expected energy of the flow state and the expected energy of the state estimation error using time-varying feedback gains for three cases, each of which including the effect of sensor noise:

(i) *Non-zero initial conditions with zero external disturbances* (dot-dashed curves): the expected energy of the state estimation error follows an initial transient, eventually tending exponentially to zero at the decay rate of the least-stable eigenmode of $A + LC$ since there is no additional excitation. In all flows considered, the expected energy of

the state estimation error is rapidly reduced to over two orders of magnitude below the expected energy of the flow state.

(ii) *Non-zero external disturbances with zero initial conditions* (dashed curves): the expected energy of the estimation error monotonically increases towards a statistical steady state. In the flow considered at wavenumber pair $\{0, 2\}$, the expected energy of the state estimation error rapidly approaches a value close to two orders of magnitude below the expected energy of the flow state, indicating effective estimator convergence. In the flows considered at wavenumber pairs $\{1, 1\}$ and $\{1, 0\}$, however, the expected energy of the state estimation error is nearly as large as the expected energy of the flow state itself, indicating poor convergence of the estimator in these particular flows. This issue is discussed in §3.2.

(iii) *Both non-zero initial conditions and non-zero external disturbances* (solid curves): as expected, owing to the linearity of the system and the additive effects of the stochastic inputs on the expected energy of the system, this case is given precisely by the sum of cases (i) and (ii).

It is also worth noting that the transient in the expected energy of the state estimation error is not only of lower amplitude, but is typically much faster than the transient in the expected energy of the flow state.

Figure 4 shows how the peak and statistical steady state of the expected energy of the flow state and state estimation error depend on the wavenumber pair, quantifying the effects seen in figure 1 for a range of different wavenumbers.

3.2. *The difficulty of detecting structures in the centre of the channel with wall sensors*

The reason the estimator discussed in the previous section fails to converge effectively in the flows at wavenumber pairs $\{1, 1\}$ and $\{1, 0\}$ when external disturbances are present is interesting. Bewley & Liu (1998, hereinafter referred to as BL98), studied extensively the Kalman filter problem in the present flow system for the following two cases:

case (i): $Re = 10\,000$, $\{k_x, k_z\} = \{1, 0\}$,
case (ii): $Re = 5000$, $\{k_x, k_z\} = \{0, 2\}$.

As shown in figure 1(*b*) of BL98, the leading eigenvectors of A in the $\{1, 0\}$ case include several 'centre' modes with nearly zero support near the wall†. These modes, which are absent in the $\{0, 2\}$ case, would be continuously excited by the external disturbances, and are nearly impossible to detect with wall measurements even if the sensor noise is very low. To quantify this notion, the corresponding 'modal observation residuals' g_κ are tabulated for both cases in tables 1 and 2 of BL98.

Because of the presence of these nearly unobservable centre modes, the estimation problem is inherently difficult at certain wavenumber pairs when both external disturbances and sensor noise are present. Thus, the failure of the Kalman filter developed here to converge accurately for the externally disturbed flows in the $\{1, 0\}$ case and the $\{1, 1\}$ case, which is characterized by similar unobservable centre modes, is a reflection of the fundamental difficulty of this estimation problem when only wall measurements are employed, and is not a shortcoming of the estimation strategy applied in the present work.

To investigate the excitation of the flow by external disturbances which do not significantly excite such centre modes, we may augment the definition of $\mathcal{M}^y$ in (2.7), which models the wall-normal distribution of the covariance of the external

---

† Note that the shapes of these modes are only weak functions of Reynolds number, so the same general comments hold true for the $Re = 3000$ case studied here.
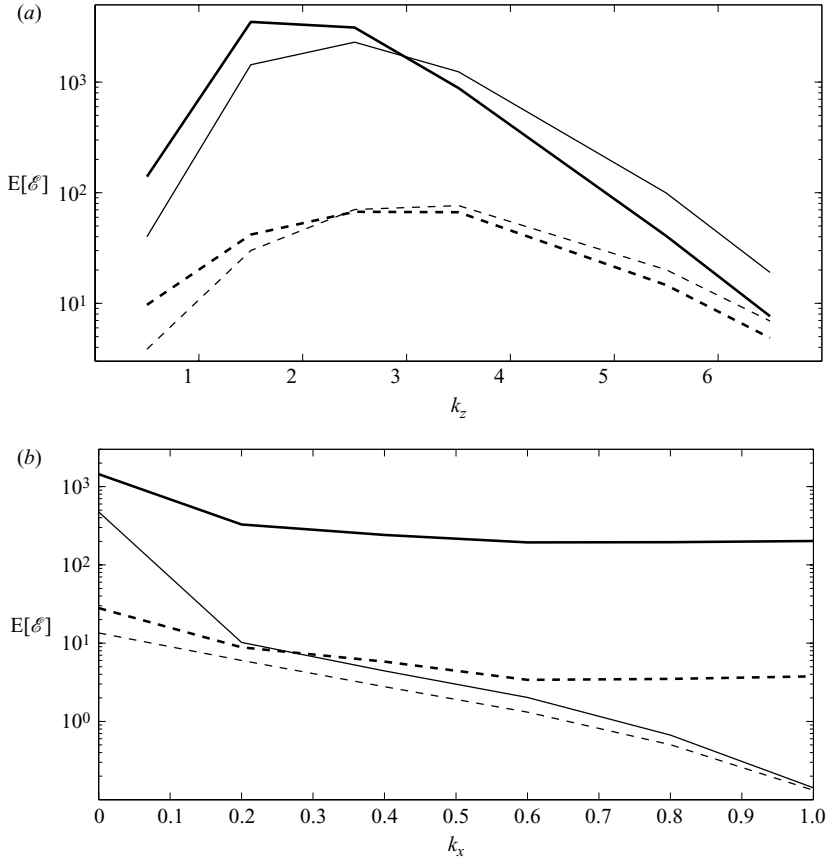
FIGURE 4. Maximum (thick lines) and statistical steady state (thin lines) of the total expected energy of the flow (solid) and the estimation error (dashed) over a range of wavenumber pairs for (*a*) $k_x = 0$ with varying k_z, and (*b*) $k_z = 1$ with varying k_x.

disturbances f, as

$$\mathscr{M}^y_{augmented} = C(p) \left(\frac{y + y'}{2} \right)^{2p} \mathscr{M}^y.$$

The parameter p may be chosen to tune the profile of the external disturbances, with uniform intensity in y if $p = 0$ or with intensity increasing near the walls if $p > 0$, as shown in figure 5. In the simulations reported here, the coefficient $C(p)$ is selected such that the total expected energy of the flow is identical in each case.

The effect of this biasing of the external disturbances towards the walls is plotted in figure 6. For the three wavenumber pairs tested, figure 6 illustrates the wall-normal distribution of the expected energy of both the flow and the estimation error at statistical steady state. The flow is forced both with the external disturbance with $p = 0$ (solid lines) and $p = 5$ (dashed lines).

For the wavenumber pair $\{0, 2\}$, the biasing of the external disturbance towards the walls has relatively little effect. In both cases tested, most of the energy of the resulting flow perturbation is located in the region of high shear, as explained by the lift-up effect. This perturbation is easily detected by the sensors on the walls, so the corresponding expected energy of the estimation error is relatively small.
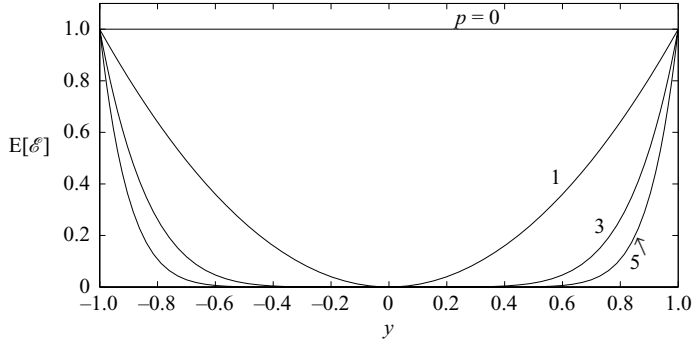
FIGURE 5. The wall-normal distribution of the variance in the augmented form of the external disturbance parameterization. Four cases are shown, corresponding to $p = 0, 1, 3$ and 5.
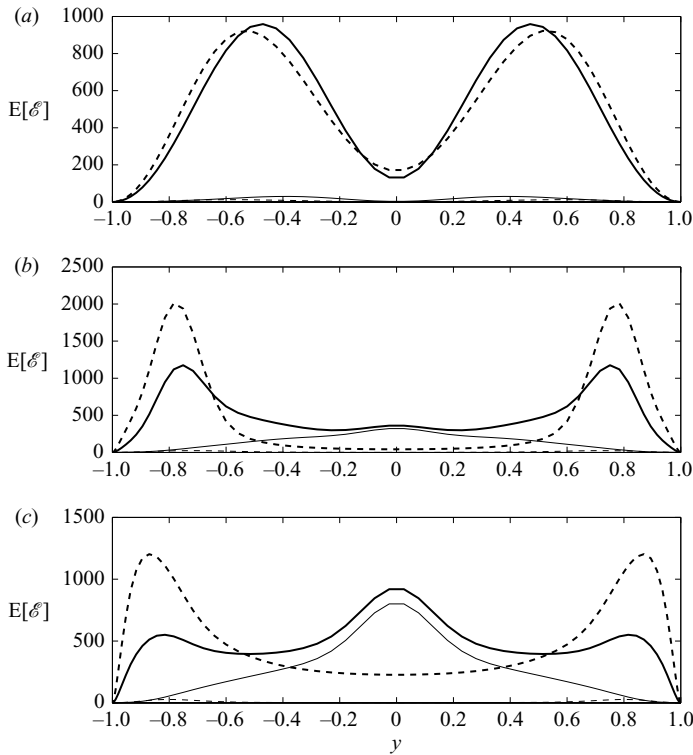

FIGURE 6. The distribution in y of the expected energy at statistical steady state of the flow (thick lines) and the estimation error (thin lines) for three wavenumber pairs: (a) $\{0, 2\}$, (b) $\{1, 1\}$, and (c) $\{1, 0\}$, and for two different wall-normal distributions of the external perturbations: $p = 0$ (solid) and $p = 5$ (dashed).

For the wavenumber pair $\{1, 0\}$, on the other hand, the biasing of the external disturbance towards the walls has a relatively strong influence on where the expected energy of the flow is located. When excitation is present in the centre of the channel (for $p = 0$), it is seen that the expected energy of the flow is relatively large near the centre of the channel. In this case, the estimator performance is poor, and the value of the expected energy of the estimation error is relatively large, especially near the centre of the channel. On the other hand, when the excitation is focused

$\{k_x, k_z\}$	$\{0, 2\}$	$\{1, 1\}$	$\{1, 0\}$
$p = 0$	28.8	289.5	548.4
$p = 1$	26.4	112.0	178.4
$p = 3$	16.3	38.3	43.8
$p = 5$	12.4	17.9	16.7

TABLE 1. The total expected energy of the estimation error at statistical steady state for three wavenumber pairs and four wall-normal distributions of the variance of the external disturbances. For each case, the magnitude of the external disturbances was scaled so that the total expected energy of the flow was 1000.

near the walls of the channel (for $p = 5$), the so-called 'centre modes' are not excited, and the estimator performance is very substantially improved, with the expected energy of the estimation error in this case being almost zero.

The characteristics of the case at wavenumber pair $\{1, 1\}$ are essentially intermediate between the two other cases, at $\{1, 0\}$ and $\{0, 2\}$.

These results are further reinforced in table 1, where the total expected energy of the estimation error is tabulated for $p = 0, 1, 3$ and 5. When the external disturbances are uniformly distributed across the channel (for $p = 0$), the estimator performance is substantially degraded for the $\{1, 0\}$ and, to a lesser extent, the $\{1, 1\}$ cases as compared to the $\{0, 2\}$ case, as already seen in figure 6. As the excitation is focused closer to the walls (that is, as p is increased), the estimator performance is substantially improved, as the nearly unobservable centre modes are no longer excited.

The flow structures that typically play the dominant role in the transition process (and, thus, the flow structures which we are most interested in estimating accurately in the present work) are elongated in the streamwise direction. That is, the modes of maximum concern in the transition process are the highly non-normal modes in the neighbourhood of $\{k_x, k_z\} = \{0, 2\}$. Fortunately, this is the wavenumber regime that is not characterized by the problematical centre modes that are difficult to estimate based on wall measurements alone. Thus, the estimator developed and tested here appears to be promising for estimating the components of the state that are most relevant to the transition problem even though this estimator is incapable of detecting the so-called centre modes. It is also significant to point out that, to model the effects of wall roughness in linearized Navier–Stokes models, it is common practice to tune the parameterization of the external disturbances to focus them near the wall, as done here for large values of p. In this setting, the resulting flow disturbances are estimated well at all wavenumber pairs, as reflected in table 1.

3.3. *The utility of time-varying gains in the estimator*

The feedback gains $\boldsymbol{L}$ determined by the Kalman filter, computed according to (2.13a)–(2.13b), are inherently a function of time. Thus, as stated previously, in order to minimize the trace of $\boldsymbol{P}(t)$ during the transient which ensues after the estimator is turned on, it is necessary to use time-varying feedback gains. However, for large times, $\boldsymbol{P}(t)$ and $\boldsymbol{L}(t)$ eventually approach constants as the estimation error approaches statistical steady state. Thus, if one is not interested in minimizing this transient, one can simply apply constant feedback gains designed to minimize the expected energy of the state estimation error at statistical steady state.

It is interesting to compare the possible utility of time-varying gains for the control and estimation problems. Consider first the problems of optimal control and optimal
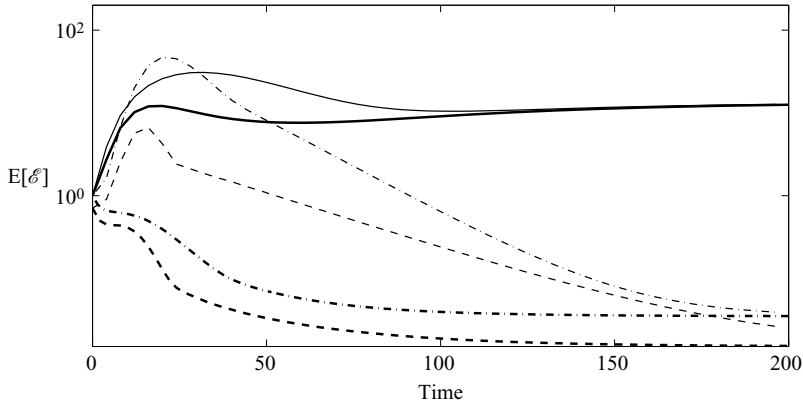
FIGURE 7. Comparison of the expected energy of the estimation error using the time-varying gains (thick lines) and constant gains (thin lines) for three wavenumber pairs: $\{0, 2\}$ solid, $\{1, 1\}$ dash-dot and $\{1, 0\}$ dash.

estimation over the finite time horizon $[0, T]$. As already seen, the optimal estimation (Kalman filter) problem is solved by a DRE that marches forward in time from $t = 0$ to $t = T$. On the other hand, the optimal control problem is solved by a (closely related) DRE that marches backward in time, from $t = T$ to $t = 0$. For time-invariant systems over a long time horizon (that is, for large T), the resulting feedback gains for the estimation problem exhibit a transient near $t = 0$ and approach a constant for the remainder of the march towards $t = T$, whereas the resulting feedback gains for the control problem exhibit a transient near $t = T$ and approach a constant for the remainder of the march towards $t = 0$. In the limit that $T \to \infty$, the transient in the gains in the control problem becomes unimportant; however, the transient in the gains in the estimation problem is still significant, especially if one is concerned with how rapidly the estimator converges after the estimator is turned on. Failure to appreciate this point can lead to the implementation of constant-gain estimators which do not converge as rapidly as one might desire.

In our previous work on dynamic compensation (Högberg *et al.* 2003), constant feedback gains for both the control and estimation problems were used, taking no account of the transient due to the initial condition in the estimator. The full-state feedback control problem was found to be solved successfully with this approach for a large number of relevant flow cases. However, the state estimation problem was not found to be solved effectively by this approach, and was left as an important open problem.

It is now clear that we cannot expect optimal estimator performance during the initial transient when using constant estimation gains if the initial condition has a significant effect on the flow. This can be seen in figure 7, where the evolution of the expected energy of the estimation error is plotted for the case of constant gains (thin lines) and the time-varying gains (thick lines). Both the constant and the time-varying gains give identical expected energy of the estimation error at large times, but the peak in the expected energy of the estimation error at short times is substantially diminished when the time-varying gains are employed. By taking the covariance of the initial condition into account, the use of the time-varying gains gives us a direct means of leveraging any knowledge we might have about the expected structure of the initial conditions in the flow case of interest.
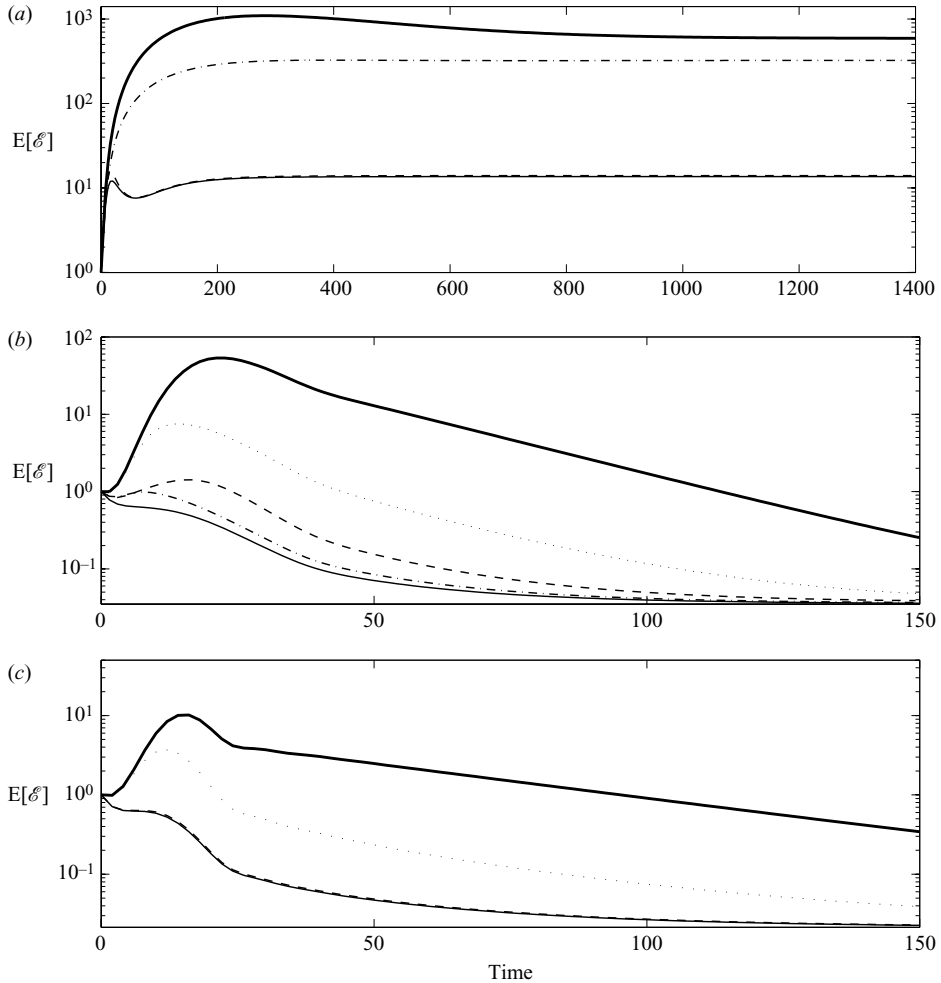
FIGURE 8. Expected energy of the flow (solid thick line) and estimation error when (solid thin line) all measurements are used, (dashed line) only measurements of τ_x are used, (dot-dashed line) only measurements of τ_z are used, and (dotted line) only measurements of wall pressure are used, at the wavenumber pairs (a) $\{0, 2\}$, (b) $\{1, 1\}$, and (c) $\{1, 0\}$. Note that the thin dotted line for $\{0, 2\}$ lies under the thick solid line.

3.4. *Relative importance of the different measured quantities*

As described in §1, the new disturbance parameterization proposed in the present work allows us now to feed back into the estimator all three types of measurements available at the wall, that is, the streamwise skin friction τ_x, the spanwise skin friction τ_z, and the wall pressure p. Figure 8 explores the relative importance of each of these individual measurements in the convergence of the estimator for the three wavenumber pairs studied previously. It is seen that the measurement of τ_x is the most significant for the estimator convergence for wavenumber pairs corresponding to streamwise elongated structures; as mentioned in the last paragraph of §3.2, we might consider these modes as the ones of maximum concern in the early stages of transition. Physically, we might say that, in this case, the estimator can leverage the strong streamwise skin friction footprint associated with the streamwise streaks
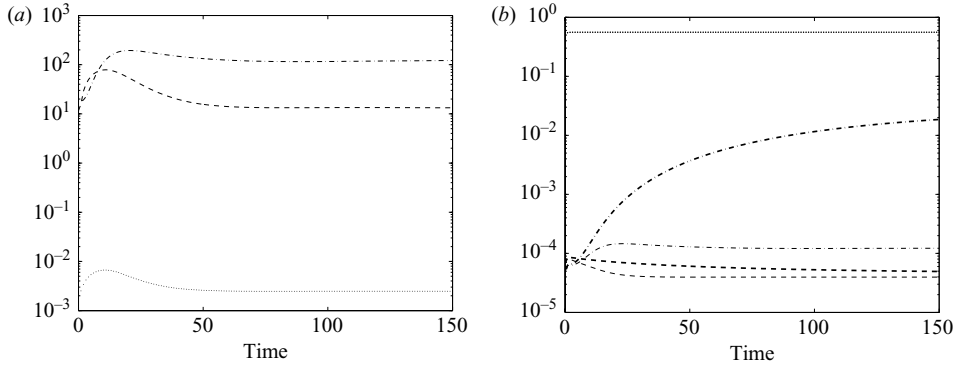
FIGURE 9. Time evolution of the peak absolute value of the gains and the variance of the measurements for the wavenumber pair $\{0, 2\}$. (*a*) Peak absolute value of the gains for the measurements of (dot-dashed) τ_x, (dashed) τ_z, and (dotted) wall pressure. (*b*) Variance of the measured signal (thick lines) and the measurement error (thin lines), with same line types as in (*a*).

created be the lift-up of low-momentum fluid by low-amplitude streamwise vortices. With the present parameterization (with a relatively high expected noise variance for the pressure measurement), the pressure measurement did not contribute as significantly as the other measurements to the estimation performance.

The evolution in time of the peak amplitudes of the feedback gains for the three different types of measurements, as well as the variance of the measured signals (that is, the expected value of the measurement signal squared), is depicted in figure 9 for the wavenumber pair $\{0, 2\}$. It is seen that the transient in the feedback gains due to the effects of the initial conditions is clearly significant.

3.5. *The effectiveness of freezing selected gains based on the unsteady solution of the DRE*

The present section attempts to give some practical insight into the behaviour of selected feedback gains chosen from snapshots of the full solution of the DRE. To this end, the expected energy of the estimation error when using constant gains that were determined from snapshots of the unsteady solution to the DRE is illustrated in figure 10. It is seen that, when gains from early in this time evolution are used, the early stages of the transient are estimated effectively, but there is increased error in the estimate as statistical steady state is approached. When gains from later in this time evolution are used, the estimate of the transient is degraded, but the estimate of the statistical steady state is significantly improved.

4. Physical-space characterization

In the previous section, the estimator was tested in the linear setting in Fourier space at individual wavenumber pairs. In this section, we inverse transform the gains computed on a large array of wavenumber pairs to obtain spatially localized convolution kernels in physical space (§4.1). We then investigate the estimation (in physical space) of two flows of interest, one at very small amplitude, in which nonlinear effects may be neglected (§4.2), and one at a finite amplitude, in which nonlinear effects are significant (§4.3).
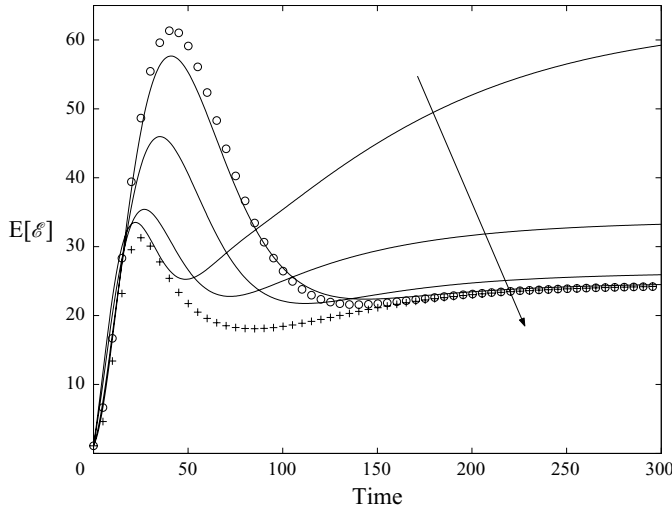
FIGURE 10. Energy of the expected estimation error for gains selected from the time-varying solution to the DRE and applied as constant-gain feedback, tested at the wavenumber pair $\{0, 2\}$. Gains are selected from times 20, 40, 60 and 80 (solid lines, with later times in the direction of the arrow), as compared with the (constant) solution of the ARE ($\circ$) and the full (time-varying) solution of the DRE ($+$).

4.1. *Physical-space feedback convolution kernels*

The feedback gains for the estimator, as formulated in §2 and tested at individual wavenumber pairs $\{k_x, k_z\}_{mn}$ in §3, are functions of the wall-normal coordinate y. By computing such feedback gains on a large array of wavenumber pairs and then performing an inverse Fourier transform in x and z, three-dimensional (physical-space) feedback convolution kernels are obtained. Such convolution kernels relate the measurement at a given sensor location on the wall to the forcing of the estimator model in the vicinity of that point, and eventually decay exponentially with distance far from the corresponding sensor. For further discussion of the interpretation of such convolution kernels, see Bewley (2001) and Högberg *et al.* (2003).

The results presented in this section were computed with $p = 0$, i.e. assuming a constant amplitude of the external disturbance forcing in the wall-normal direction.

4.1.1. *Time variation of the kernels*

To illustrate the time variation of the kernels computed via solution of the DRE, the evolution in time of the kernels corresponding to the measurement of the streamwise skin friction is shown in figure 11. Note that the shape of this kernel varies rapidly near $t = 0$, then gradually approaches a steady state. Also note that, near $t = 0$, the kernel is similar in its streamwise and spanwise extent, but, as time evolves, the kernel becomes elongated in its streamwise extent. This is consistent with the fact that streamwise elongated structures are persistent in time and typically dominate such flows.

4.1.2. *Steady-state shapes of the kernels*

The time-varying kernels computed via the solution of the DRE eventually converge to a steady state. Figure 12 shows these steady-state shapes for each of the three measurement and the two evolution equations. Note the close correspondence between
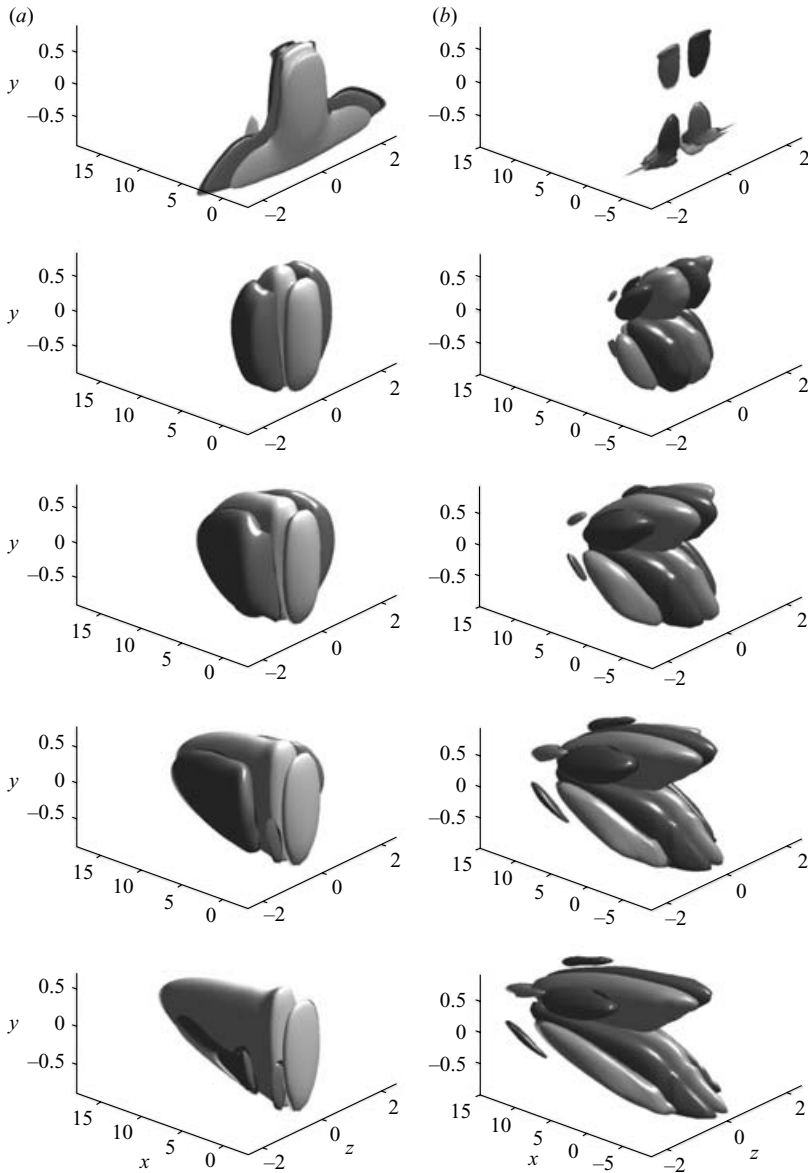
FIGURE 11. The time-varying kernel for times (top to bottom) $t = 0$, 15, 30, 45 and 60, relating the streamwise component of the shear stress measurement at the point $\{x = 0, \ y = -1, \ z = 0\}$ on the wall to the estimator forcing on the interior of the domain for the evolution equation for the estimate of (a) v and (b) η. Visualized are positive (dark) and negative (light) isosurfaces with isovalues of $\pm 5\%$ of the maximum amplitude for each kernel illustrated.

the steady-state kernels for the τ_x measurement in figure 12 and the corresponding kernels at $t = 60$ in figure 11.

It is important to note that the spatial extent of the convolution kernels is related, to some degree, to the correlation length scales chosen during the disturbance parameterization defining the estimation problem. Specifically, the parameters d_x, d_y and d_z parameterizing the correlation length scales of the disturbances in §2.4.2 have a direct
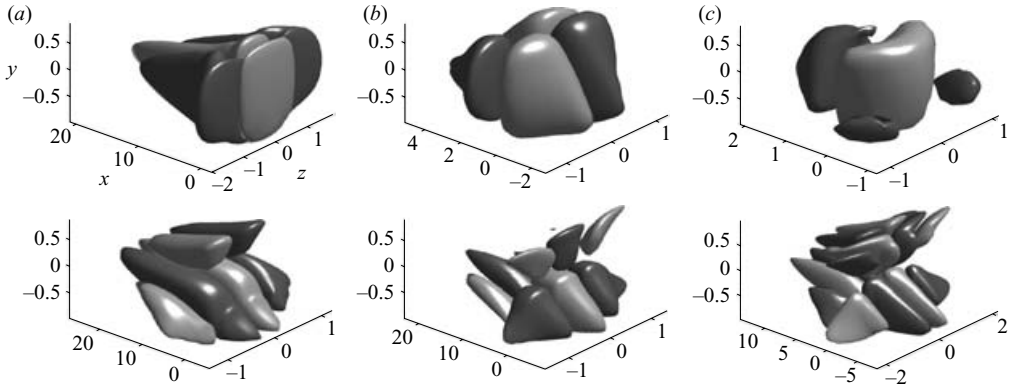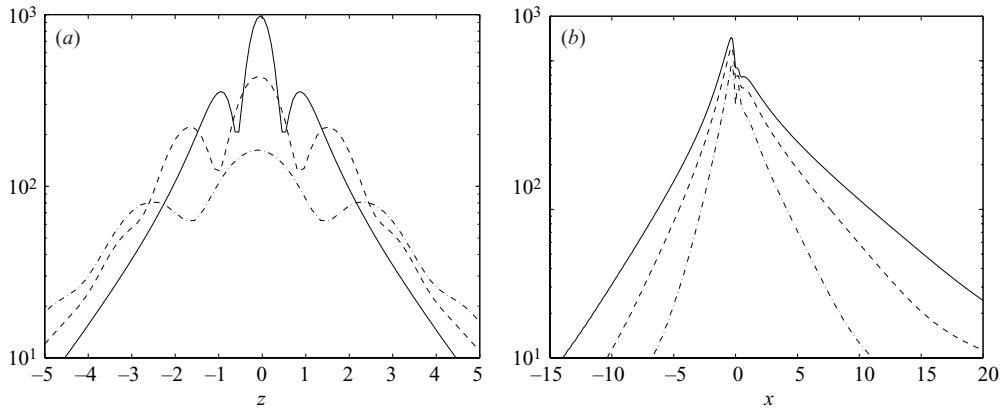
FIGURE 12. The steady-state convolution kernels relating the (a) τ_x, (b) τ_z and (c) p measurements at the point $\{x=0,\ y=-1,\ z=0\}$ on the wall to the estimator forcing on the interior of the domain for the evolution equation for the estimate of v (top) and η (bottom). Visualized are positive (dark) and negative (light) isosurfaces with isovalues of $\pm 5\%$ of the maximum amplitude for each kernel illustrated.

FIGURE 13. Decay of the pressure kernel forcing the streamwise velocity component of the state estimate, (a) integrated in the streamwise and wall normal direction for (solid) $d_x = d_z = 0.2$, (dashed) 0.7, and (dot-dashed) 1.3, and (b) integrated in the spanwise and wall-normal directions for (solid) $Re = 3000$, (dashed) 2000, (dot-dashed) 1000.

effect on the spatial extent of the present kernels. For example, figure 13(a) shows, for three different values of d_z, the spanwise extent of the pressure kernel forcing the streamwise velocity component of the state estimate, integrated in the streamwise and wall-normal directions. It is clear that, when designing feedback for disturbances which are more 'spread out' in the spanwise direction (that is, disturbances with greater two-point correlation length scales in the spanwise direction), the corresponding convolution kernel has a broader spanwise extent. It is also seen that this broader kernel has a lower peak amplitude, since the corresponding forcing is more distributed.

The streamwise extent of the kernel is less sensitive to the streamwise correlation length scale of the disturbances, but is a strong function of the Reynolds number. In a flow with a higher Reynolds number, the effect of flow advection is more pronounced, and information from wall sensors can be related to the interior flow structures responsible for this wall footprint that have since advected further downstream. This

effect can be clearly seen in figure 13(b), which shows the same kernel as in figure 13(a), but integrated in the spanwise and cross-flow directions for three different Reynolds numbers.

4.2. *Estimation of an infinitesimal localized flow perturbation*

The localized flow perturbation studied by Henningson, Lundbladh & Johansson (1993) is now used to test the convergence of the estimator in physical space. In this section, we will consider the direct numerical simulation of an infinitesimal flow perturbation, so that nonlinear effects in this section can effectively be neglected.

Recall that the estimator initializes the state estimate as zero; that is, it assumes no *a priori* knowledge of the location of the initial flow perturbation. In the following, we explore different models for the assumed covariance of the initial estimation error by varying the design parameter c_2 in (2.6). This parameter effectively reflects our level of confidence in our knowledge of the relevant statistical properties of the initial conditions, ranging from 0.05 (little specific knowledge of the statistical properties of the initial conditions) to 1 (accurate knowledge of these statistics, but no knowledge of the actual location of the initial flow perturbation). For the simulations reported here, the exact initial condition of the flow perturbation, described below, is used as the 'specific' component s in the parameterization of the initial covariance of the estimation error, $P(0)$, for the purpose of the computation of the feedback kernels.

The external disturbance forcing of the flow considered in this section is taken as zero, so the resulting simulation might be characterized as a 'deterministic' case with no stochastic forcing. The initial condition of the flow considered in this section consists of an axisymmetric disturbance of the form

$$\left.\begin{aligned}
\psi &= \tfrac{1}{2}\varepsilon f(y)r^2 \mathrm{e}^{-(r/l)^2}, \\
f(y) &= (1+y)^2(1-y)^5, \\
(u, v, w) &= \left(-\frac{x}{r^2}\psi_y, \frac{1}{r}\psi_r, -\frac{z}{r^2}\psi_y\right).
\end{aligned}\right\} \tag{4.1}$$

Here (x, y, z) are the streamwise, wall-normal and spanwise coordinates, respectively, $r^2 = x^2 + z^2$, and (u, v, w) are the corresponding velocity components. The horizontal extent of this perturbation may be adjusted with the parameter l, which is set equal to 1 for the presented simulations so that the maximum energy of the initial flow perturbation in Fourier space is at the wavenumber pairs showing the greatest transient energy growth, as illustrated in figure 14. The parameter ε scaling the amplitude of the initial flow perturbation is taken as 0.001.

Five different estimators, as formulated in the previous sections with feedback gains computed by selecting $c_2 = 0.05$, 0.1, 0.25, 0.5 and 1, respectively, were tested on the problem of estimating this flow. It can be seen in figure 15 that the variation of c_2 between 1 and 0.25 had a relatively small effect on the resulting estimator performance, and that all four of the estimators tested in this range significantly outperformed the estimator that used only the steady-state kernels (dashed line), which does not depend on the parameterization of the statistics of the initial conditions. On the other hand, the estimator in the case with $c_2 = 0.05$ significantly underperformed the others, indicating that, when no useful information is available concerning the statistics of the initial conditions, it might be better simply to use the steady-state kernels computed via solution of the ARE.

Figure 16 visualizes the evolution of this flow perturbation (figure 16a) as it evolves from the initial conditions provided, as well as the evolution of the state estimate
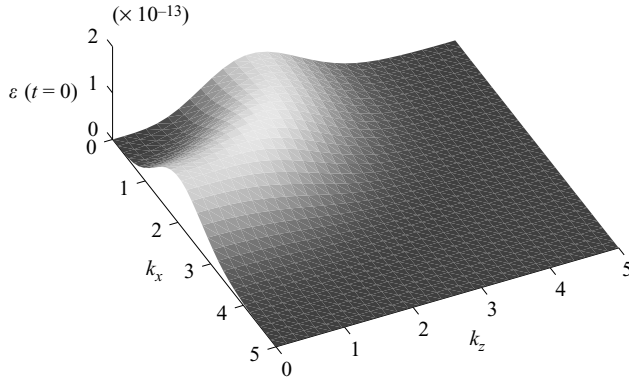
FIGURE 14. Energy content (in Fourier space) of the initial condition for the case studied in §§4.2 and 4.3.
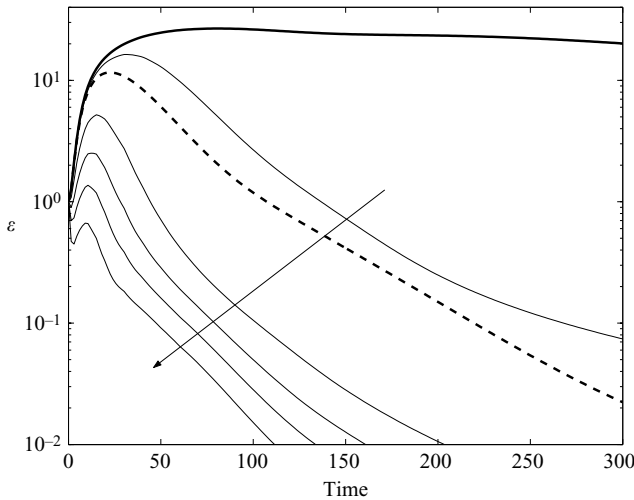

FIGURE 15. The time evolution of the energy of an infinitesimal localized flow perturbation (thick solid line) and the energy of the estimation error of the same flow using (dashed line) the steady-state kernels determined from the solution of the ARE as well as (thin solid lines) a gain scheduled set of kernels computed using values of $c_2 = 0.05$, 0.1, 0.25, 0.5 and 1, increasing in the direction of the arrow. Note that the energy $\mathscr{E}$ has been normalized by energy of the initial flow perturbation.

(figure 16*b*) as it evolves from the initial condition of zero and is forced by the feedback of the measurement error term as formulated in (2.9)–(2.10). It is seen that, by time $t = 60$, all of the major features of the flow are apparently reproduced well by the state estimate. Additionally, as seen in figure 15, the time $t = 60$ is rather early in the evolution of the flow perturbation – the energy of the flow perturbation is still growing substantially at this point, while the energy of the state estimation error is by now decaying exponentially, indicating successful convergence of the estimator.

4.3. *Estimation of a finite-amplitude flow perturbation*

We now test the same estimator as used previously on the problem of estimating a flow with the same initial conditions as considered in §4.2, but with an initial amplitude now almost an order of magnitude larger, such that nonlinear effects play
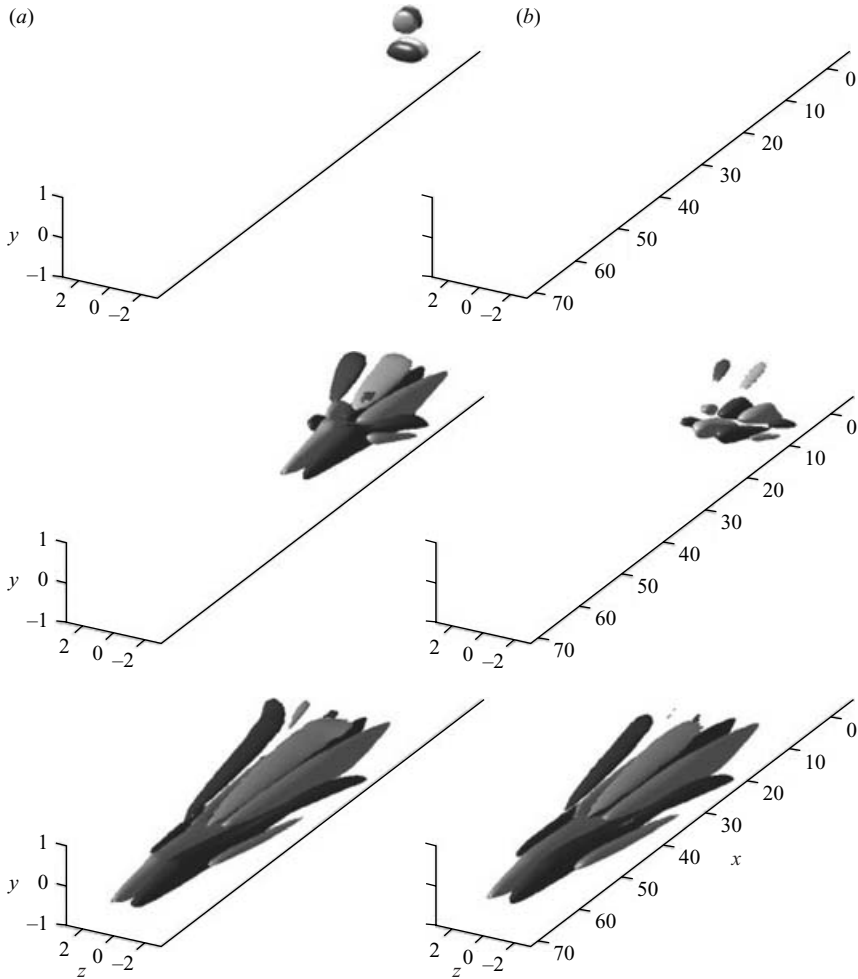
FIGURE 16. Evolution of (*a*) a localized disturbance to the state and (*b*) the corresponding state estimate at time $t = 0$ (top), $t = 20$ (middle), and $t = 60$ (bottom), computed with $c_2 = 0.08$. Visualized are positive (light) and negative (dark) isosurfaces of the streamwise component of the velocity. The isovalues are $\pm 10\%$ of the maximum streamwise velocity of the flow during the time interval shown.

a significant role. We take $\varepsilon = 0.00828$, which corresponds to a maximum wall normal velocity of 0.0117 at $t = 0$ (this is approximately $\approx 1.2\%$ of the maximum velocity of the mean flow).

As in §4.2, the direct numerical simulation reported here used the code described in Lundbladh, Henningson & Johansson (1992), which uses a pseudo-spectral scheme with Fourier, Chebychev and Fourier techniques in the streamwise, wall-normal and spanwise directions, respectively. The time advancement was a third-order Runge–Kutta method for the nonlinear terms and a second-order Crank–Nicolson method for the linear terms. The box size is $48 \times 2 \times 24$ and the grid resolution is $96 \times 65 \times 192$.

As mentioned in the third paragraph of §3, the estimator used in this work has already been designed to handle well the leading-order effects of nonlinearity. Since we know from Henningson *et al.* (1993) that nonlinear effects will be most pronounced at wavenumber pairs with lower k_x and higher k_z than the initial conditions, we have
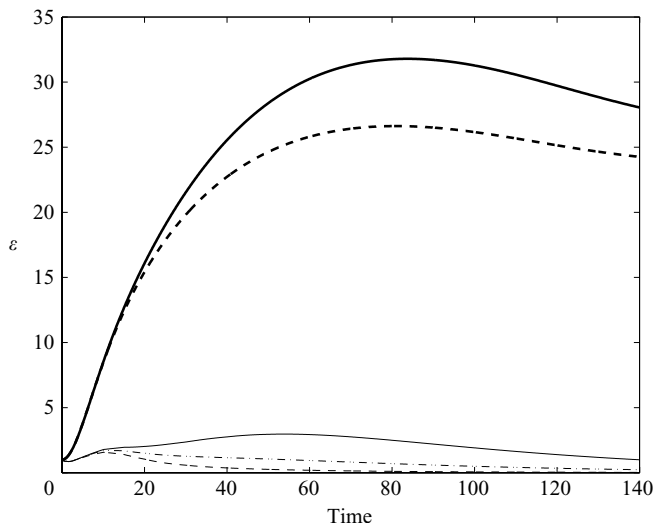
FIGURE 17. Evolution of the normalized flow energy (thick lines) and normalized estimation error energy (thin lines) for the case with moderate-amplitude initial conditions (solid) and low-amplitude initial conditions (dashed). The evolution of the normalized estimation error energy for the extended Kalman filter in the case with moderate-amplitude initial conditions is also plotted (thin dot-dashed line), illustrating a significant improvement as compared with the performance of the corresponding Kalman filter (thin solid line) when nonlinearities are significant.

tuned the covariance of the external disturbance model upon which the estimator is based to account specifically for unmodelled dynamics at these wavenumbers, as depicted in figure 2. The model for the external disturbances accounts here for a forcing of higher amplitude than for the tests on single wavenumber pairs of §3, with $d_a = 0.68$, and located closer to the walls, with $p = 1$. With this choice of parameters, the expected flow energy grows due to the initial condition, and continues to grow due to the forcing f, in a way similar to the nonlinear evolution of the flow.

The evolution of the energy of the state and the estimation error for both the moderate-amplitude case (§4.3) and the small-amplitude case (§4.2) are plotted in figure 17. To facilitate comparison, all curves have been normalized to unity at $t = 0$. Note the significant difference in the normalized energy evolution of the state in the two cases considered (compare the thick solid line and the thick dashed line); this reflects the significant effects of nonlinearities in the moderate amplitude case. For both cases, the initial stage of the evolution (during which nonlinear effects are fairly small in both cases) is estimated well (thin lines). As the moderate-amplitude perturbation evolves and its amplitude grows, nonlinear effects become significant, and the performance of the linear estimator (thin solid line) is degraded as compared with the performance of the linear estimator in the small-amplitude case (thin dashed line).

The Kalman filter is an 'optimal' estimator (in several rigorous respects – see Anderson & Moore (1979) for a detailed discussion) in the linear setting. As seen in figure 17 and discussed in the previous paragraph, when a Kalman filter is applied to a nonlinear system, its performance is typically degraded, owing to the fact that the linear model upon which the Kalman filter is based does not include all the terms of the (nonlinear) equation governing the actual system. A common (though somewhat

ad hoc) patch which partially accounts for this deficiency is to reintroduce the system nonlinearity to the estimator model after the Kalman filter is designed. This approach is called an extended Kalman filter. This type of estimator is identical to the Kalman filter except for the presence of the system's nonlinearity in the estimator model. This addition makes some sense: if the estimate of the state happens to match the actual state, no feedback from measurements is required for the extended Kalman filter to track the actual flow state. This is not the case for the standard (linear) Kalman filter. As seen clearly in figure 17, the extended Kalman filter (thin dot-dashed line) enjoys a substantial performance improvement compared with its standard Kalman filter counterpart (the thin solid line) for estimating finite-amplitude flow perturbations when nonlinearities in the system model are significant.

5. Conclusions

A canonical feedback-control problem in fluid mechanics, which undoubtedly sets the stage for several follow-on flow-control problems that incorporate greater geometric complexity, is the feedback control of a near-wall flow system based on limited noisy measurements from flush wall-mounted sensors in order to stabilize the flow and inhibit transition to turbulence. In such problems, it is natural to apply model-based linear control theory, as the equations of motion of the system are well known and the linearization of these equations is valid, at least during the early stages of the transition process when all flow perturbations are small. The mathematical framework for the linear control theory we have chosen to apply in the present study, commonly called 'optimal' or '$\mathscr{H}_2$' control theory, is well known in both the finite- and infinite-dimensional setting. However, the fact that the flow system is infinite dimensional and that regularity issues play a very subtle role in the well posedness of this control problem in the infinite-dimensional setting, compounded by the fact that the theory of well posedness of the equations of motion of the system of interest (that is, the three-dimensional Navier–Stokes equation) is not yet even complete, leads to some peculiar challenges in the well-posed framing and subsequent numerical solution of this challenging flow-control problem.

Via the so-called separation principle, such linearized flow-control problems in the optimal setting break up into two independent subproblems: control of the flow with whatever actuators are available based on full state information, and estimation of the full flow state with whatever sensors are available. Once both subproblems are solved effectively, they may be combined to develop a dynamic compensator to control the flow system using limited actuation authority (with, for example, actuators mounted on the walls) based only on limited noisy measurements of the flow (with, for example, sensors mounted on the walls). In previous work, excellent results had been obtained on the full-state feedback control problem, but certain unresolved difficulties remained on the estimation problem. The present work thus focused exclusively on the estimation problem.

The first important development in this work was the introduction of a physically relevant parameterization of the external disturbances acting on the system that converges upon refinement of the numerical grid. This disturbance parameterization is fairly generic, and can easily be used to give an insight into the initial conditions likely to be encountered in a given flow (for example, Tollmien–Schlichting (TS) waves, streaks, or streamwise vortices). Also, the disturbance parameterization can be tuned in order to modify (at least, to some degree) the spatial extent of the resulting convolution kernels.

Using this disturbance parameterization, together with appropriate parameterizations of the initial conditions and the measurement noise, feedback gains for the estimation problem were computed (using a efficient Chandrasekhar method) for the near-wall flow system in Fourier space on a large array of (decoupled) wavenumber pairs $\{k_x, k_z\}$, then inversed transformed to obtain physical-space convolution kernels. The improved disturbance parameterization proposed in this study facilitated, for the first time, the computation of measurement feedback gains in the discretized problem that converged upon grid refinement (and thus are relevant for the infinite-dimensional problem upon which the numerical problem solved in the computer was derived) for all three types of measurements that are available on the wall (that is, streamwise and spanwise wall skin friction and wall pressure).

The second significant development in this work was the recognition that for the problem of transition control, though time-invariant feedback gains (computed from a corresponding algebraic Riccati equation) are sufficient for the full-state feedback control problem, time-varying feedback gains (computed from a differential Riccati equation) are necessary for the estimation problem in order to minimize the initial transient in the estimation error when the estimator is turned on.

The estimator feedback rules that resulted from these two developments were tested extensively both in Fourier space (in the linearized setting) and in physical space (in direct numerical simulations of both infinitesimal and finite-amplitude disturbances for which the effects of nonlinearity are significant). The estimator was shown to perform well for all cases studied except when the external disturbances excited centre modes, which can happen sometimes for wavenumber pairs with relatively large streamwise component (that is, for modes which are relatively large in their spanwise extent). Fortunately, it was recognized that such cases are not the primary cases of interest in most transition scenarios. It was also found that, when the flow perturbations were large enough that the nonlinearities of the system were significant, an extended Kalman filter which incorporated the system nonlinearity in the estimator model outperformed the standard (linear) Kalman filter.

Part 2 of this study will give a summary of recent work considering the extension of such estimation strategies to the problem of fully developed near-wall turbulence.

REFERENCES

ANDERSON, B. & MOORE, J. 1979 *Optimal Filtering*. Prentice-Hall.

BALAKRISHNAN, A. V. 1976 *Applied Functional Analysis*. Springer.

BEWLEY, T. R. 2001 Flow control: new challenges for a new renaissance. *Prog. Aerospace Sci.* **37**, 21–58.

BEWLEY, T. R. & LIU, S. 1998 Optimal and robust control and estimation of linear paths to transition. *J. Fluid Mech.* **365**, 305–349.

BEWLEY, T. R. & PROTAS, B. 2003 Skin friction and pressure: the 'footprints' of turbulence. *Physica D* **196**, 28–44.

GUNZBERGER, M. D. 1996 *Perspectives in Flow Control and Optimization*. SIAM.

HANIFI, A., SCHMID, P. J. & HENNINGSON, D. S. 1996 Transient growth in compressible boundary layer flow. *Phys. Fluids* **8**, 826–836.

HENNINGSON, D. S., LUNDBLADH, A. & JOHANSSON, A. V. 1993 A mechanism for bypass transition from localized disturbances in wall-bounded shear flow. *J. Fluid Mech.* **250**, 169–207.

HÖGBERG, M., BEWLEY, T. R. & HENNINGSON, D. S. 2003 Linear feedback control and estimation of transition in plane channel flow. *J. Fluid Mech.* **481**, 149–175.

HUANG, W. & SLOAN, D. M. 1993 The pseudo-spectral method for solving differential eigenvalue problems. *J. Comput. Phys.* **111**, 399–409.

JOSHI, S. S., SPEYER, J. L. & KIM, J. 1999 Finite dimensional optimal control of Poiseuille flow. *J. Guid. Control Dyn.* **22**, 340.

JOVANOVIĆ, M. & BAMIEH, B. 2001*a* Modelling flow statistics using the linearized Navier–Stokes equations. *Proc. 40'th IEEE Conf. on Decision and Control, FL.*

JOVANOVIĆ, M. & BAMIEH, B. 2001*b* The spatio-temporal impulse response of the linearized Navier–Stokes equations. *Proc. Am. Control Conf.*

KAILATH, T. 1973 Some new algorithms for recursive estimation in constant linear systems. *IEEE Trans. Inform. Theory* **19**, 750–760.

KIM, J. 2003 Control of turbulent boundary layers. *Phys. Fluids* **15**, 1093–1105.

KIM, J. & LIM, J. 2000 A linear process in wall-bounded turbulent shear flows. *Phys. Fluids* **12**, 1885–1888.

LAUB, A. 1991 *Invariant Subspace Methods for the Numerical Solution of Riccati Equations*. Springer.

LEE, C., KIM, J., BABCOCK, C. & GOODMAN, R. 1997 Application of neural network to turbulence control for drag reduction. *Phys. Fluids* **9**, 1740–1747.

LEWIS, F. L. & SYRMOS, V. L. 1995 *Optimal Control*. Wiley-Interscience.

LUNDBLADH, A., HENNINGSON, D. & JOHANSSON, A. 1992 An efficient spectral integration method for the solution of the Navier–Stokes equations. *Tech. Rep.* Aeronautical Research Institute of Sweden, Bromma.

SCHMID, P. J. & HENNINGSON, D. S. 2001 *Stability and Transition in Shear Flows*. Springer.

THOMAS, A. S. W. 1990 Active wave control of boundary-layer transition. In *Viscous Drag Reduction in Boundary Layers* (ed. D. M. Bushnell & J. N. Hefner), *Progress in Astronautics and Aeronautics*, vol. 123. American Institute of Aeronautics and Astronautics Washington, DC.

WEIDEMAN, J. A. C. & REDDY, S. C. 2000 A MATLAB differentiation matrix suite. *ACM Trans. Math. Software* **26**, 465–519.